AIMS Mathematics, 10(2): 4374–4411.
DOI: 10.3934/math.2025202
Received: 24 December 2024
Revised: 09 February 2025
Accepted: 18 February 2025
Published: 28 February 2025

http://www.aimspress.com/journal/Math

Research article

Novel solitary wave solutions of the (3+1)–dimensional nonlinear Schrödinger equation with generalized Kudryashov self–phase modulation

Nafissa Toureche Trouba[1,2], Mohamed E. M. Alngar[3], Reham M. A. Shohib[4], Haitham A. Mahmoud[5], Yakup Yildirim[6,7,*], Huiying Xu[1,*] and Xinzhong Zhu[1,8]

[1] School of Computer Science and Technology, Zhejiang Normal University, Jinhua, 321004, China
[2] Zhejiang Institute of Photoelectronics, Jinhua, Zhejiang 321004, China
[3] Department of Mathematics Education, Faculty of Education & Arts, Sohar University, Sohar 3111, Oman
[4] Basic Science Department, Higher Institute of Management Sciences & Foreign Trade, Cairo, 379, Egypt
[5] Industrial Engineering Department, College of Engineering, King Saud University, Riyadh 11421, Saudi Arabia
[6] Department of Computer Engineering, Biruni University, Istanbul–34010, Turkey
[7] Mathematics Research Center, Near East University, 99138 Nicosia, Cyprus
[8] College of Computer Science and Artificial Intelligence, Wenzhou University, Wenzhou 325035, China

* **Correspondence:** Email: yakupyildirim110@gmail.com; xhy@zjnu.edu.cn.

Abstract: This paper investigates the (3+1)-dimensional nonlinear Schrödinger equation, incorporating cross-spatial dispersion and a generalized form of Kudryashov's self-phase modulation. Using the generalized Jacobi elliptic method, we systematically derive novel soliton solutions expressed in terms of Jacobi elliptic and Weierstrass elliptic functions, providing deeper insights into wave dynamics in nonlinear optical media. The obtained solutions exhibit diverse structural transformations governed by the parameter (n) known as full nonlinearity, encompassing optical bullet solutions, optical domain wall solutions, singular solitons, and periodic solutions. Furthermore, we discuss the potential experimental realization of these solitonic structures in ultrafast fiber lasers and nonlinear optical systems, drawing connections to recent experimental findings. To facilitate a comprehensive understanding of their physical properties, we present detailed three-dimensional (3D), two-dimensional (2D), and contour visualizations, highlighting the interplay among dispersion, nonlinearity, and self-modulation effects. These results offer new perspectives on soliton interactions and have significant implications for optical communication, signal processing, and nonlinear wave phenomena.

Keywords: novel solitons; cross-spatio-dispersion; generalized Jacobi elliptic method
Mathematics Subject Classification: 35Q55, 35Q60, 35Q61

1. Introduction

Nonlinear optics is a vibrant and dynamic field within optical science that pushes beyond the constraints of linear optical phenomena [1,2]. It delves into the complex interplay between intense light and matter, giving rise to a plethora of intriguing nonlinear effects. These effects present unparalleled opportunities for manipulating and controlling light, with applications spanning various disciplines including telecommunications, imaging, and signal processing. Among the captivating nonlinear phenomena are optical bullets and domain walls [3,4]. These are localized structures characterized by unique properties that have versatile applications. Optical bullets and domain walls are particularly significant due to their potential impact on telecommunications and signal processing technologies. The behavior and stability of optical solitons, dromions, bullets, and domain walls are determined by the delicate balance between chromatic dispersion (CD) and self-phase modulation (SPM) [5,6]. CD refers to the phenomenon where different wavelengths of light travel at different speeds through a medium, while SPM is the change in the phase of an optical wave caused by its interaction with a nonlinear medium. Understanding the interplay between CD and SPM is crucial for controlling the dynamics of optical structures. The concept of SPM, initially introduced by Kudryashov, has emerged as a pivotal aspect of nonlinear optics [7–9]. It provides a powerful mechanism for altering the dynamics of an optical system by modulating the phase of the medium in response to intense optical fields. Building upon prior research [10–13], recent studies have focused on exploring cross-spatial dispersive effects to uncover new behaviors of optical soliton solutions. By formulating a novel Schrödinger equation in three dimensions, researchers have expanded the theoretical framework of nonlinear optics, opening up new avenues for investigation and application [14–19]. In this expanded framework, CD extends along three spatial directions, leading to pairwise cross-spatial dispersion effects and a total of six dispersive effects [20–22]. Additionally, Kudryashov's innovative form of SPM introduces eight coupled SPM effects alongside the dispersion effects in the Schrödinger equation [23,24]. The primary goal of recent research endeavors is to utilize the generalized Jacobi elliptic method [25,26] to derive solutions for various optical structures in (3+1) dimensions. These structures include Jacobi elliptic functions, optical bullets, domain walls, singular solitons, Weierstrass elliptic functions, and periodic structures. By employing advanced mathematical techniques, researchers aim to deepen our understanding of light propagation in complex media and uncover new insights into the behavior of optical structures. The contributions of these studies extend beyond theoretical advancements. They include the extension of the Schrödinger equation to (3+1) dimensions, the development of a comprehensive dispersion model, the introduction of a novel SPM effect, and the exploration of the coupling between dispersion and SPM effects. The insights provided by these investigations not only enrich our foundational understanding of nonlinear optical systems but also hold significant promise for practical applications in ultrafast all-optical signal processing. By harnessing the unique properties of optical bullets, researchers aim to advance high-speed data transmission and storage technologies, paving the way for innovative

developments in telecommunications and information technology.

In this study, our focus centers on delving into the intricacies of the extended (3+1)-dimensional nonlinear Schrödinger equation (NLSE), a fundamental mathematical framework that governs the behavior of optical systems in complex media. The NLSE is a cornerstone in nonlinear optics, providing a powerful tool for understanding the propagation of intense light through nonlinear materials. The extension to (3+1) dimensions is a significant advancement that allows for a more comprehensive modeling of optical phenomena. By incorporating an additional spatial dimension, researchers can capture the full complexity of light propagation in three-dimensional (3D) space, along with the temporal dimension. Central to our investigation is the incorporation of cross-spatio-dispersion effects into the NLSE formulation. Spatio-dispersion refers to the spatial variation of dispersion characteristics within a medium. In other words, different regions of space may exhibit varying degrees of dispersion, influencing the behavior of optical waves as they propagate. Moreover, we integrate Kudryashov's proposed form of SPM into the NLSE framework. SPM, a nonlinear optical effect, describes the modulation of the phase of an optical wave as it interacts with a nonlinear medium. Kudryashov's proposed form of SPM introduces additional complexity and richness to the NLSE model, enabling a more accurate representation of real-world optical systems. Our approach builds upon prior works, which have laid the groundwork for extending the NLSE to (3+1) dimensions and incorporating cross spatio-dispersion effects and Kudryashov's form of SPM. These works have demonstrated the feasibility and importance of considering these factors in understanding optical phenomena in multidimensional space. By investigating the extended (3+1)-dimensional NLSE with cross-spatio-dispersion and Kudryashov's SPM, we aim to gain deeper insights into the behavior of optical structures such as optical bullets, domain walls, and solitons. Through mathematical analysis and numerical simulations, we seek to elucidate how these structures evolve and interact in three-dimensional space-time, taking into account the intricate interplay among dispersion, nonlinearity, and spatial variation. Lastly, our study contributes to the advancement of nonlinear optics by refining theoretical models and enhancing our understanding of light–matter interactions in multidimensional media. The insights gained from this investigation may have far-reaching implications for various applications, including optical communication, signal processing, and quantum information processing.

The model equation is introduced below:

$$\begin{aligned} &iQ_t - \Big(a_1 Q_{xx} + a_2 Q_{yy} + a_3 Q_{zz} + 2a_4 Q_{xy} - 2a_5 Q_{xz} - 2a_6 Q_{yx} \Big) \\ &+ \Big(b_1 |Q|^{-n} + b_2 |Q|^{-2n} + b_3 |Q|^{-3n} + b_4 |Q|^{-4n} + c_1 |Q|^{n} + c_2 |Q|^{2n} + c_3 |Q|^{3n} + c_4 |Q|^{4n} \Big) Q = 0. \end{aligned} \tag{1}$$

In the context of the extended (3+1)-dimensional NLSE with cross-spatio-dispersion and Kudryashov's proposed form of SPM, the function $Q(x, y, z, t)$ serves as a crucial component. This function represents complex-valued wave profiles, with t representing the temporal variable and x, y, and z representing the spatial variables. The imaginary unit i is defined as $i^2 = -1$, allowing for complex-valued representations of wave profiles. Within the NLSE framework, the coefficients a_j (where j ranges from 1 to 6), b_k, and c_k (where k ranges from 1 to 4) are constants that play significant roles in shaping the behavior of the optical system. These coefficients govern various aspects of the optical properties, including CD and SPM. The coefficient a_1 specifically represents CD, a phenomenon where different wavelengths of light propagate at different speeds through a medium.

This dispersion is influenced by the coefficients a_2, a_3, a_4, a_5, and a_6, which contribute to cross-spatio-dispersion effects. Cross-spatio-dispersion refers to the spatial variation of dispersion characteristics across different dimensions, adding complexity to the dispersion profile and affecting how optical waves propagate in multidimensional space [20–22]. These terms account for interactions between spatial coordinates, reflecting the coupling between different dispersion directions. In particular:

- $a_2 Q_{yy}$ and $a_3 Q_{zz}$ represent second-order dispersion along the y- and z-axes, similar to the conventional chromatic dispersion term $a_1 Q_{xx}$.
- $a_4 Q_{xy}$, $a_5 Q_{xz}$, and $a_6 Q_{yz}$ introduce mixed partial derivatives, which describe how dispersion in one direction influences another. These terms are crucial for modeling complex wave interactions in an isotropic or in homogeneous optical media.

The numerical coefficients (such as 1 and 2) appearing in front of these terms in Eq (1) originate from the derivation process of the equation from higher-order NLSE formulations. These prefactors ensure the correct scaling of each term, preserving the fundamental balance between dispersion and nonlinearity. Specifically, the factors of 2 in front of some cross-terms arise due to the symmetry properties of second-order mixed derivatives:

$$Q_{xy} = Q_{yx}, \quad Q_{xz} = Q_{zx}, \quad Q_{yz} = Q_{zy}.$$

This symmetry leads to the standard form of Eq (1), where the cross-dispersion terms appear with appropriate coefficients. Additionally, the coefficients b_k and c_k contribute to SPM, a nonlinear optical effect where the phase of an optical wave is modulated as it interacts with a nonlinear medium. These coefficients govern the strength and nature of the SPM effect, influencing how the phase of the optical wave evolves over time and space. In Eq (1), the terms involving b_k and c_k describe the nonlinear response of the medium [7,9]. SPM is a nonlinear optical effect where the phase of an optical wave is modulated due to the intensity-dependent refractive index of the medium. In the context of our model, both the positive and negative powers of Q contribute to this effect for the following reasons.

1) Nonlinear refractive index modulation:

   - The positive power terms (e.g., $c_1|Q|^n, c_2|Q|^{2n}$, etc.) represent the conventional self-focusing effect, where the refractive index increases with the field intensity. This is a well-known feature of materials exhibiting Kerr-type nonlinearity.
   - The negative power terms (e.g., $b_1|Q|^{-n}, b_2|Q|^{-2n}$, etc.) introduce additional nonlinear effects, which can be interpreted as higher-order nonlinear contributions, typically seen in some specially engineered optical materials where low-intensity regions experience different phase shifts.

2) Balance between self-focusing and defocusing effects:

   - The coexistence of both positive and negative power terms implies a competition between self-focusing and defocusing effects, which significantly alters the wave dynamics. The presence of inverse power nonlinearities can lead to novel soliton solutions, including singular solitons and periodic structures.

- This interplay enables a more generalized form of SPM, allowing for a richer variety of wave interactions, including those relevant to optical bullets and domain walls.

3) Generalized Kudryashov SPM model:

- The equation incorporates Kudryashov's extended SPM framework, where nonlinearity is not solely dependent on direct power laws but includes inverse nonlinear terms as well.
- This generalization allows the model to describe complex nonlinear interactions in optical systems, particularly in non-Kerr media, where deviations from standard cubic nonlinearity arise.

Lastly, the nonlinearity index n denotes the power law parameter, which characterizes the nonlinearity of the medium. The value of n determines the degree of nonlinearity in the NLSE, impacting the formation and stability of optical structures such as solitons, domain walls, and optical bullets. Therefore, the coefficients a_j, b_k, and c_k in the extended NLSE with cross-spatio-dispersion and Kudryashov's SPM form the foundational elements that govern the behavior of optical waves in multidimensional space. Understanding the roles of these coefficients is essential for analyzing and predicting the dynamics of nonlinear optical phenomena and their applications in various fields such as telecommunications, imaging, and signal processing.

The study of nonlinear wave dynamics in higher-dimensional systems is crucial for understanding various physical phenomena. In this work, we focus on the (3+1)-dimensional nonlinear Schrödinger equation, which is relevant to soliton propagation in optical fibers and Bose–Einstein condensates. Our research introduces new solutions and explores the effects of modulation and dispersion on soliton behavior.

We derive novel Jacobi elliptic and Weierstrass elliptic function solutions for the (3+1)-dimensional nonlinear Schrödinger equation, providing new insights into soliton dynamics. Additionally, we present a generalized Kudryashov self-phase modulation (SPM) model that includes both focusing and defocusing effects, offering a more comprehensive description of nonlinear wave behavior. We also examine the role of cross-spatial dispersion terms in shaping soliton structures, contributing to a deeper understanding of soliton interactions in multidimensional optical systems. Finally, we connect our theoretical findings to recent experimental studies on soliton interactions in ultrafast fiber lasers, emphasizing the practical implications of our results. These advancements enhance our understanding of soliton dynamics in multidimensional systems and have potential applications in optical technologies.

The structure of this paper is carefully designed to provide a systematic exploration of the extended (3+1)-dimensional NLSE with cross-spatio-dispersion and Kudryashov's proposed form of SPM. Each section of the paper contributes distinctively to our understanding of the model and its implications. Section 2 delves into an extensive mathematical analysis of the extended NLSE. It involves deriving the equations governing chromatic dispersion, self-phase modulation, and nonlinearity, as well as exploring the implications of cross-spatio-dispersion on the behavior of optical waves. This analysis provides the theoretical foundation for the subsequent sections. In Section 3, the paper describes the integration method employed to solve the extended NLSE. The generalized Jacobi elliptic method is introduced as a powerful mathematical technique for finding analytical solutions to nonlinear partial differential equations. The section explains the principles of the method and its application to the NLSE. Building upon the theoretical framework established in the previous

sections, Section 4 focuses on the practical implementation of the integration method to the model equation derived in Section 2. The goal is to derive novel soliton solutions that capture the behavior of optical structures such as optical bullets and domain walls in multidimensional space. In Section 5, the paper presents the results obtained via the integration method and provides comprehensive plots illustrating the behavior of optical solitons, domain walls, and other structures predicted by the model. The discussion interprets these results, highlighting key findings, comparing them with existing literature, and exploring their implications for nonlinear optics and related fields. Finally, Section 6 concludes by summarizing the main findings and contributions of the study. It discusses the significance of the results in advancing our understanding of nonlinear optical systems and outlines potential avenues for future research. The section emphasizes the importance of the extended NLSE with cross-spatio-dispersion and Kudryashov's SPM in addressing complex optical phenomena and its relevance to practical applications in telecommunications, signal processing, and beyond.

2. Mathematical analysis

In order to address this objective, we propose that the exact solution to Eq (1) can be articulated in the following manner:

$$Q(x,y,z,t) = \Phi(\zeta)\exp[iF(x,y,z,t)], \tag{2}$$

where $\Phi(\zeta) = \Phi$, and $F(x,y,z,t)$ represent real-valued functions, satisfying the condition:

$$\zeta = \beta_1 x + \beta_2 y + \beta_3 z - vt, \;\; F(x,y,z,t) = -\kappa_1 x - \kappa_2 y - \kappa_3 z + \omega t + \zeta_0. \tag{3}$$

Here, the symbol v denotes the velocity of the soliton, along the x, y, and z axes, while the wave numbers are symbolized by κ_1, κ_2, and κ_3, respectively. Additionally, ζ_0 represents the phase constant, and ω signifies the frequency. In the context of an optical bullet, β_1, β_2, and β_3 denote the directional ratios, indicating the widths along the three spatial dimensions. Upon substituting Eqs (2) and (3) into Eq (1) and separating it into its real and imaginary components, we have:

$$\begin{aligned}
&\Re : -\left(a_1\beta_1^2 + a_2\beta_2^2 + a_3\beta_3^2 + 2a_4\beta_1\beta_2 - 2a_5\beta_1\beta_3 - 2a_6\beta_2\beta_3\right)\Phi'' \\
&+\left(-\omega + a_1\kappa_1^2 + a_2\kappa_2^2 + a_3\kappa_3^2 + 2a_4\kappa_1\kappa_2 - 2a_5\kappa_1\kappa_3 - 2a_6\kappa_2\kappa_3\right)\Phi \\
&+b_1\Phi^{1-n} + b_2\Phi^{1-2n} + b_3\Phi^{1-3n} + b_4\Phi^{1-4n} + c_1\Phi^{1+n} + c_2\Phi^{1+2n} + c_3\Phi^{1+3n} + c_4\Phi^{1+4n} = 0,
\end{aligned} \tag{4}$$

and

$$\Im : \left[-v + 2\beta_1(a_1\kappa_1 + a_4\kappa_2 - a_5\kappa_3) + 2\beta_2(a_2\kappa_2 + a_4\kappa_1 - a_6\kappa_3) + 2\beta_3(a_3\kappa_3 - a_5\kappa_1 - a_6\kappa_2)\right]\Phi' = 0. \tag{5}$$

Based on Eq (5), one can infer

$$v = 2\beta_1(a_1\kappa_1 + a_4\kappa_2 - a_5\kappa_3) + 2\beta_2(a_2\kappa_2 + a_4\kappa_1 - a_6\kappa_3) + 2\beta_3(a_3\kappa_3 - a_5\kappa_1 - a_6\kappa_2). \tag{6}$$

To obtain solutions in a closed form, we consider the following transformation:

$$\Phi(\zeta) = \left[U(\zeta)\right]^{\frac{1}{2n}}, \tag{7}$$

assuming that $U(\zeta)$ is positive. By substituting Eq (7) into Eq (4), we obtain:

$$2n\Pi_1\ U(\zeta)U''(\zeta) + (1-2n)\,\Pi_1\ \left[U'(\zeta)\right]^2 + 4n^2\,(\Pi_2-\omega)\ U^2(\zeta) + 4n^2 b_1\ U^{\frac{3}{2}}(\zeta) + 4n^2 b_2\ U(\zeta)$$
$$+4n^2 b_3\ U^{\frac{1}{2}}(\zeta) + 4n^2 b_4 + 4n^2 c_1\ U^{\frac{5}{2}}(\zeta) + 4n^2 c_2\ U^3(\zeta) + 4n^2 c_3\ U^{\frac{7}{2}}(\zeta) + 4n^2 c_4\ U^4(\zeta) = 0, \tag{8}$$

where

$$\Pi_1 = -\left(a_1\beta_1^2 + a_2\beta_2^2 + a_3\beta_3^2 + 2a_4\beta_1\beta_2 - 2a_5\beta_1\beta_3 - 2a_6\beta_2\beta_3\right),$$
$$\Pi_2 = a_1\kappa_1^2 + a_2\kappa_2^2 + a_3\kappa_3^2 + 2a_4\kappa_1\kappa_2 - 2a_5\kappa_1\kappa_3 - 2a_6\kappa_2\kappa_3. \tag{9}$$

To guarantee integrability, it is crucial to carefully select

$$b_1 = b_3 = c_1 = c_3 = 0. \tag{10}$$

Hence, Eq (8) becomes

$$2n\Pi_1\ U(\zeta)U''(\zeta) + (1-2n)\,\Pi_1\ \left[U'(\zeta)\right]^2 + 4n^2\,(\Pi_2-\omega)\ U^2(\zeta)$$
$$+4n^2 b_2\ U(\zeta) + 4n^2 b_4 + 4n^2 c_2\ U^3(\zeta) + 4n^2 c_4\ U^4(\zeta) = 0. \tag{11}$$

3. Generalized Jacobi elliptic method

We suggest that Eq (11) has the following formal solution:

$$U(\zeta) = \gamma_0 + \sum_{j=1}^{N} \gamma_j\ \varphi^j(\zeta), \tag{12}$$

where N is a positive integer belonging to the set of positive integers ($\mathbb{Z}^+$), and γ_j (where j ranges from 0 to N) is a constant, with the condition that $\gamma_N \neq 0$. Additionally, $\varphi(\zeta)$ is the solution of the equation:

$$\varphi'^2(\zeta) = \chi_0 + \chi_2\ \varphi^2(\zeta) + \chi_4\ \varphi^4(\zeta). \tag{13}$$

The constants χ_0, χ_2, and χ_4 are parameters. It is widely acknowledged that Eq (13) allows the following solutions to be expressed in terms of generalized Jacobian elliptic functions (GJEFs).

Type 1. $\chi_0 = \dfrac{m^2(m^2-1)\chi_2^2}{(2m^2-1)^2\chi_4}$, $0 < m < 1$, and

$$\varphi(\zeta) = \begin{cases} \pm m\sqrt{-\dfrac{\chi_2}{(2m^2-1)\chi_4}}\,\mathrm{cn}\left(\sqrt{\dfrac{\chi_2}{2m^2-1}}\zeta\right), & \left(2m^2-1\right)\chi_2 > 0, \chi_4 < 0, \\ \pm\sqrt{\dfrac{\left(1-m^2\right)\chi_2}{(2m^2-1)\chi_4}}\,\mathrm{nc}\left(\sqrt{\dfrac{\chi_2}{2m^2-1}}\zeta\right), & \left(2m^2-1\right)\chi_2 > 0, \chi_4 > 0, \\ \pm m\sqrt{-\dfrac{\left(1-m^2\right)\chi_2}{(2m^2-1)\chi_4}}\,\mathrm{sd}\left(\sqrt{\dfrac{\chi_2}{2m^2-1}}\zeta\right), & \left(2m^2-1\right)\chi_2 > 0, \chi_4 < 0, \\ \pm\sqrt{\dfrac{\chi_2}{(2m^2-1)\chi_4}}\,\mathrm{ds}\left(\sqrt{\dfrac{\chi_2}{2m^2-1}}\zeta\right), & \left(2m^2-1\right)\chi_2 > 0, \chi_4 > 0. \end{cases} \tag{14}$$

Type 2. $\chi_0 = \dfrac{m^2\chi_2^2}{(1+m^2)^2\chi_4}$, $0 < m < 1$, and

$$\varphi(\zeta) = \begin{cases} \pm m\sqrt{-\dfrac{\chi_2}{(1+m^2)\chi_4}}\,\mathrm{sn}\left(\sqrt{-\dfrac{\chi_2}{1+m^2}}\zeta\right), & \chi_2 < 0, \chi_4 > 0, \\ \pm\sqrt{-\dfrac{\chi_2}{(1+m^2)\chi_4}}\,\mathrm{ns}\left(\sqrt{-\dfrac{\chi_2}{1+m^2}}\zeta\right), & \chi_2 < 0, \chi_4 > 0, \\ \pm m\sqrt{-\dfrac{\chi_2}{(1+m^2)\chi_4}}\,\mathrm{cd}\left(\sqrt{-\dfrac{\chi_2}{1+m^2}}\zeta\right), & \chi_2 < 0, \chi_4 > 0, \\ \pm\sqrt{-\dfrac{\chi_2}{(1+m^2)\chi_4}}\,\mathrm{dc}\left(\sqrt{-\dfrac{\chi_2}{1+m^2}}\zeta\right), & \chi_2 < 0, \chi_4 > 0. \end{cases} \tag{15}$$

Type 3. $\chi_0 = \dfrac{(1-m^2)\chi_2^2}{(2-m^2)^2\chi_4}$, $0 < m < 1$, and

$$\varphi(\zeta) = \begin{cases} \pm\sqrt{-\dfrac{\chi_2}{(2-m^2)\chi_4}}\,\mathrm{dn}\left(\sqrt{\dfrac{\chi_2}{2-m^2}}\zeta\right), & \chi_2 > 0, \chi_4 < 0, \\ \pm\sqrt{-\dfrac{\left(1-m^2\right)\chi_2}{(2-m^2)\chi_4}}\,\mathrm{nd}\left(\sqrt{\dfrac{\chi_2}{2-m^2}}\zeta\right), & \chi_2 < 0, \chi_4 < 0, \\ \pm\sqrt{\dfrac{\chi_2}{(2-m^2)\chi_4}}\,\mathrm{cs}\left(\sqrt{\dfrac{\chi_2}{2-m^2}}\zeta\right), & \chi_2 > 0, \chi_4 > 0, \\ \pm\sqrt{\dfrac{\left(1-m^2\right)\chi_2}{(2-m^2)\chi_4}}\,\mathrm{sc}\left(\sqrt{\dfrac{\chi_2}{2-m^2}}\zeta\right), & \chi_2 > 0, \chi_4 > 0. \end{cases} \tag{16}$$

Type 4. $\chi_0 = \dfrac{(1-m^2)^2\chi_2^2}{4\left(1+m^2\right)^2\chi_4}$, $0 < m < 1$, and

$$\varphi(\zeta) = \begin{cases} \pm\sqrt{-\dfrac{\chi_2}{2\left(1+m^2\right)\chi_4}}\left[m\mathrm{cn}\left(\sqrt{\dfrac{2\chi_2}{1+m^2}}\zeta\right) \pm \mathrm{dn}\left(\sqrt{\dfrac{2\chi_2}{1+m^2}}\zeta\right)\right], & \chi_2 > 0, \chi_4 < 0, \\ \pm\sqrt{-\dfrac{\left(1-m^2\right)\chi_2}{2\left(1+m^2\right)\chi_4}}\left[m\mathrm{sd}\left(\sqrt{\dfrac{2\chi_2}{1+m^2}}\zeta\right) \pm \mathrm{nd}\left(\sqrt{\dfrac{2\chi_2}{1+m^2}}\zeta\right)\right], & \chi_2 > 0, \chi_4 < 0, \\ \pm\sqrt{\dfrac{\left(1-m^2\right)\chi_2}{2\left(1+m^2\right)\chi_4}}\left[\mathrm{nc}\left(\sqrt{\dfrac{2\chi_2}{1+m^2}}\zeta\right) \pm \mathrm{sc}\left(\sqrt{\dfrac{2\chi_2}{1+m^2}}\zeta\right)\right], & \chi_2 > 0, \chi_4 > 0, \\ \pm\sqrt{\dfrac{\left(1-m^2\right)\chi_2}{2\left(1+m^2\right)\chi_4}}\mathrm{cn}\left(\sqrt{\dfrac{2\chi_2}{1+m^2}}\zeta\right)\left[1 \pm \mathrm{sn}\left(\sqrt{\dfrac{2\chi_2}{1+m^2}}\zeta\right)\right]^{-1}, & \chi_2 > 0, \chi_4 > 0. \end{cases} \tag{17}$$

Type 5. $\chi_0 = \dfrac{m^4\chi_2^2}{4\left(2-m^2\right)^2\chi_4}$, $0 < m < 1$, and

$$\varphi(\zeta) = \sqrt{-\frac{\chi_2}{2\left(2-m^2\right)\chi_4}}\left[\sqrt{1-m^2}\mathrm{nc}\left(\sqrt{-\frac{2\chi_2}{2-m^2}}\zeta\right) \pm \mathrm{dc}\left(\sqrt{-\frac{2\chi_2}{2-m^2}}\zeta\right)\right], \quad \chi_2 < 0, \chi_4 > 0. \tag{18}$$

Type 6. Equation (13) also possesses the following solutions expressed in terms of Weierstrass elliptic functions (WEFs):

$$\varphi(\zeta) = \begin{cases} \dfrac{3\wp'(\zeta, l_2, l_3)}{\sqrt{\chi_4}\left[6\wp(\zeta, l_2, l_3) + \chi_2\right]}, & \chi_4 > 0, \\ \dfrac{\sqrt{\chi_0}\left[6\wp(\zeta, l_2, l_3) + \chi_2\right]}{3\wp'(\zeta, l_2, l_3)}, & \chi_0 > 0, \end{cases} \tag{19}$$

where

$$l_2 = \chi_0\chi_4 + \frac{\chi_2^2}{12} \text{ and } l_2 = \frac{\chi_2\left(36l_0\chi_4 - \chi_2^2\right)}{216}. \tag{20}$$

Here, $\wp(\zeta, l_2, l_3)$ denotes a WEF, and $\wp'(\zeta, l_2, l_3) = \frac{d\wp(\zeta, l_2, l_3)}{d\zeta}$. This function satisfies the equation $\wp'^2 = 4\wp^3 - l_2\wp - l_3$, where l_2 and l_3 are referred to as the invariants of the WEF.

4. Novel solitary wave solutions

By employing the balance technique between $U(\zeta)U''(\zeta)$ and $U^4(\zeta)$ as described in Eq (11), we obtain $N = 1$, resulting in the following expression for the solution:

$$U(\zeta) = \gamma_0 + \gamma_1\,\varphi(\zeta). \tag{21}$$

Incorporating Eq (21) along with Eq (12) into Eq (11), we obtain the following set of algebraic equations:

$$\left.\begin{array}{l} 4\left[c_4\gamma_0^4+c_2\gamma_0^3+(\Pi_2-\omega)\gamma_0^2+b_2\gamma_0+b_4\right]n^2-2\Pi_1\gamma_1^2 n\chi_0+\Pi_1\gamma_1^2\chi_0=0,\\ 4\left[\gamma_1^2(c_2+4c_4\gamma_0)n+\chi_4\gamma_0\Pi_1\right]n\gamma_1=0,\\ \left(4c_4n^2\gamma_1^2+2\Pi_1 n\chi_4+\Pi_1\chi_4\right)\gamma_1^2=0,\\ 8\left[16c_4\gamma_0^3+12c_2\gamma_0^2+8(\Pi_2-\omega)\gamma_0+4b_2\right]n^2\gamma_1+2n\Pi_1\gamma_0\gamma_1\chi_2=0,\\ \left[4(3c_2\gamma_0+\Pi_2-\omega+6c_4\gamma_0^2)n^2+\chi_2\Pi_1\right]\gamma_1^2=0. \end{array}\right\} \tag{22}$$

Result 1. When setting $\chi_0=\dfrac{m^2(m^2-1)\chi_2^2}{(2m^2-1)^2\chi_4}$ in Eq (22) and solving it with Maple, the following results are revealed:

$$\gamma_0=-\frac{c_2\,(2\,n+1)}{4c_4\,(n+1)},\ \gamma_0=\pm\frac{1}{2n}\sqrt{-\frac{(2\,n+1)\,\Pi_1\chi_4}{c_4}},\ \chi_2=\frac{\left[16\,(n+1)^3\,b_2c_4^2+\left(4\,n^3-3\,n-1\right)c_2^3\right]n^2}{2\,(n+1)^2\,(n-1)\,(2\,n+1)\,\Pi_1c_2c_4}, \tag{23}$$

and

$$\left.\begin{array}{l} \omega=\dfrac{4\,\,(n+1)^2\,(n-1)\,(2\,n+1)\,\Pi_2c_2c_4+8\,\,(n+1)^3\,b_2c_4^2-\left(4\,n^3-3\,n-1\right)c_2^3}{4\,(n+1)^2\,(n-1)\,(2\,n+1)\,c_2c_4},\\ b_4=\dfrac{(2\,n-1)\left\{\,(2n+1)^2(n-1)\left[32\,(n+1)^3b_2c_2^3c_4^2+(2n+1)^2(n-1)c_2^6\right]+1024(1-m^2)(n+1)^6b_2^2c_4^4\right\}}{256\left(2m^2-1\right)^2(n-1)^2(n+1)^4(2\,n+1)c_2^2c_4^3}, \end{array}\right\} \tag{24}$$

assuming that $\Pi_1\chi 4c4<0$. By integrating Eq (23) along with Eq (14) into Eq (21), it follows that Eq (1) presents the following solutions in accordance with the Jacobian elliptic function (JEF):

$$\begin{aligned} Q(x,y,z,t)=&\left[\begin{array}{l} -\frac{(2\,n+1)c_2}{4(1+n)c_4}\pm\frac{m}{2(1+n)c_4}\sqrt{\frac{16\,(1+n)^3b_2c_4^2+\left(4\,n^3-3\,n-1\right)c_2^3}{2\left(2\,m^2-1\right)(n-1)c_2}}\\ \times\,\mathrm{cn}\left(\frac{n}{(1+n)}\sqrt{\frac{16\,(1+n)^3b_2c_4^2+\left(4\,n^3-3\,n-1\right)c_2^3}{2\left(2\,m^2-1\right)(n-1)(2\,n+1)\Pi_1c_2c_4}}\,(\beta_1x+\beta_2y+\beta_3z-vt)\right) \end{array}\right]^{\frac{1}{2n}}\\ &\times\,e^{i(-\kappa_1x-\kappa_2y-\kappa_3z+\omega t+\zeta_0)}, \end{aligned} \tag{25}$$

provided that $\left(2\,m^2-1\right)c_2\left[16\,(1+n)^3\,b_2c_4^2+\left(4\,n^3-3\,n-1\right)c_2^3\right]>0$ and $\Pi_1c_4>0$.

$$\begin{aligned} Q(x,y,z,t)=&\left[\begin{array}{l} -\frac{(2\,n+1)c_2}{4(1+n)c_4}\pm\frac{1}{2(1+n)c_4}\sqrt{-\frac{\left(1-m^2\right)\left[16\,(1+n)^3b_2c_4^2+\left(4\,n^3-3\,n-1\right)c_2^3\right]}{2\left(2\,m^2-1\right)(n-1)c_2}}\\ \times\,\mathrm{nc}\left(\frac{n}{(1+n)}\sqrt{\frac{16\,(1+n)^3b_2c_4^2+\left(4\,n^3-3\,n-1\right)c_2^3}{2\left(2\,m^2-1\right)(n-1)(2\,n+1)\Pi_1c_2c_4}}\,(\beta_1x+\beta_2y+\beta_3z-vt)\right) \end{array}\right]^{\frac{1}{2n}}\\ &\times\,e^{i(-\kappa_1x-\kappa_2y-\kappa_3z+\omega t+\zeta_0)}, \end{aligned} \tag{26}$$

provided that $\left(2m^2-1\right)c_2\left[16\ (1+n)^3 b_2c_4^2+\left(4n^3-3n-1\right)c_2^3\right]<0$ and $\Pi_1 c_4<0$.

$$Q(x,y,z,t)=\left[\begin{array}{l}-\frac{(2n+1)c_2}{4(1+n)c_4}\pm\frac{m}{2(1+n)c_4}\sqrt{\frac{\left(1-m^2\right)\left[16\,(1+n)^3b_2c_4^2+\left(4n^3-3n-1\right)c_2^3\right]}{2\left(2m^2-1\right)(n-1)c_2}}\\ \times\,\mathrm{sd}\left(\frac{n}{(1+n)}\sqrt{\frac{16\,(1+n)^3b_2c_4^2+\left(4n^3-3n-1\right)c_2^3}{2\left(2m^2-1\right)(n-1)(2n+1)\Pi_1c_2c_4}}\,(\beta_1x+\beta_2y+\beta_3z-vt)\right)\end{array}\right]^{\frac{1}{2n}}\times\ e^{i(-\kappa_1x-\kappa_2y-\kappa_3z+\omega t+\zeta_0)},\tag{27}$$

provided that $\left(2m^2-1\right)c_2\left[16\ (1+n)^3 b_2c_4^2+\left(4n^3-3n-1\right)c_2^3\right]>0$ and $\Pi_1 c_4>0$.

$$Q(x,y,z,t)=\left[\begin{array}{l}-\frac{(2n+1)c_2}{4(1+n)c_4}\pm\frac{1}{2(1+n)c_4}\sqrt{-\frac{16\,(1+n)^3b_2c_4^2+\left(4n^3-3n-1\right)c_2^3}{2\left(2m^2-1\right)(n-1)c_2}}\\ \times\,\mathrm{ds}\left(\frac{n}{(1+n)}\sqrt{\frac{16\,(1+n)^3b_2c_4^2+\left(4n^3-3n-1\right)c_2^3}{2\left(2m^2-1\right)(n-1)(2n+1)\Pi_1c_2c_4}}\,(\beta_1x+\beta_2y+\beta_3z-vt)\right)\end{array}\right]^{\frac{1}{2n}}\times\ e^{i(-\kappa_1x-\kappa_2y-\kappa_3z+\omega t+\zeta_0)},\tag{28}$$

provided that $\left(2m^2-1\right)c_2\left[16\ (1+n)^3 b_2c_4^2+\left(4n^3-3n-1\right)c_2^3\right]<0$ and $\Pi_1 c_4<0$. When $m=1$ in Eqs (25) and (28), it yields the optical bullet solution and the singular soliton solution, respectively

$$Q(x,y,z,t)=\left[\begin{array}{l}-\frac{(2n+1)c_2}{4(1+n)c_4}\pm\frac{1}{2(1+n)c_4}\sqrt{\frac{16\,(1+n)^3b_2c_4^2+\left(4n^3-3n-1\right)c_2^3}{2(n-1)c_2}}\\ \times\,\mathrm{sech}\left(\frac{n}{(1+n)}\sqrt{\frac{16\,(1+n)^3b_2c_4^2+\left(4n^3-3n-1\right)c_2^3}{2(n-1)(2n+1)\Pi_1c_2c_4}}\,(\beta_1x+\beta_2y+\beta_3z-vt)\right)\end{array}\right]^{\frac{1}{2n}}\times\ e^{i(-\kappa_1x-\kappa_2y-\kappa_3z+\omega t+\zeta_0)},\tag{29}$$

and

$$Q(x,y,z,t)=\left[\begin{array}{l}-\frac{(2n+1)c_2}{4(1+n)c_4}\pm\frac{1}{2(1+n)c_4}\sqrt{-\frac{16\,(1+n)^3b_2c_4^2+\left(4n^3-3n-1\right)c_2^3}{2(n-1)c_2}}\\ \times\,\mathrm{csch}\left(\frac{n}{(1+n)}\sqrt{\frac{16\,(1+n)^3b_2c_4^2+\left(4n^3-3n-1\right)c_2^3}{2(n-1)(2n+1)\Pi_1c_2c_4}}\,(\beta_1x+\beta_2y+\beta_3z-vt)\right)\end{array}\right]^{\frac{1}{2n}}\times\ e^{i(-\kappa_1x-\kappa_2y-\kappa_3z+\omega t+\zeta_0)}.\tag{30}$$

When $m=0$ in Eqs (26) and (28), it leads to periodic solutions, which are, respectively:

$$Q(x,y,z,t)=\left[\begin{array}{l}-\frac{(2n+1)c_2}{4(1+n)c_4}\pm\frac{1}{2(1+n)c_4}\sqrt{\frac{16\,(1+n)^3b_2c_4^2+\left(4n^3-3n-1\right)c_2^3}{2(n-1)c_2}}\\ \times\,\sec\left(\frac{n}{(1+n)}\sqrt{-\frac{16\,(1+n)^3b_2c_4^2+\left(4n^3-3n-1\right)c_2^3}{2(n-1)(2n+1)\Pi_1c_2c_4}}\,(\beta_1x+\beta_2y+\beta_3z-vt)\right)\end{array}\right]^{\frac{1}{2n}}\times\ e^{i(-\kappa_1x-\kappa_2y-\kappa_3z+\omega t+\zeta_0)},\tag{31}$$

and

$$Q(x,y,z,t)=\left[\begin{array}{l}-\frac{(2n+1)c_2}{4(1+n)c_4}\pm\frac{1}{2(1+n)c_4}\sqrt{\frac{16(1+n)^3b_2c_4^2+\left(4n^3-3n-1\right)c_2^3}{2(n-1)c_2}}\\ \times\csc\left(\frac{n}{(1+n)}\sqrt{-\frac{16(1+n)^3b_2c_4^2+\left(4n^3-3n-1\right)c_2^3}{2(n-1)(2n+1)\Pi_1c_2c_4}}\left(\beta_1x+\beta_2y+\beta_3z-vt\right)\right)\end{array}\right]^{\frac{1}{2n}}\times\ e^{i(-\kappa_1x-\kappa_2y-\kappa_3z+\omega t+\zeta_0)}. \tag{32}$$

Result 2. When setting $\chi_0=\dfrac{m^2\chi_2^2}{(1+m^2)^2\chi_4}$ in Eq (22) and solving it with Maple, the resulting solution remains the same as in Eq (23), along with the emergence of the following constraint conditions:

$$\left.\begin{array}{l}\omega=\dfrac{4\ (n+1)^2(n-1)(2n+1)\Pi_2c_2c_4+8\ (n+1)^3b_2c_4^2-\left(4n^3-3n-1\right)c_2^3}{4(n+1)^2(n-1)(2n+1)c_2c_4},\\ b_4=\dfrac{(2n-1)\left\{\left(m^2-1\right)^2(2n+1)^2(n-1)\left[32(n+1)^3b_2c_2^3c_4^2+(2n+1)^2(n-1)c_2^6\right]-1024m^2(n+1)^6b_2^2c_4^4\right\}}{256\left(m^2+1\right)^2(n-1)^2(n+1)^4(2n+1)c_2^2c_4^3}.\end{array}\right\} \tag{33}$$

By incorporating Eq (23) along with Eq (15) into Eq (21), it follows that Eq (1) presents the following solutions in accordance with the JEF

$$Q(x,y,z,t)=\left[\begin{array}{l}-\frac{(2n+1)c_2}{4(1+n)c_4}\pm\frac{m}{2(1+n)c_4}\sqrt{\frac{16(1+n)^3b_2c_4^2+\left(4n^3-3n-1\right)c_2^3}{2\left(1+m^2\right)(n-1)c_2}}\\ \times\mathrm{sn}\left(\frac{n}{(1+n)}\sqrt{-\frac{16(1+n)^3b_2c_4^2+\left(4n^3-3n-1\right)c_2^3}{2\left(m^2+1\right)(n-1)(2n+1)\Pi_1c_2c_4}}\left(\beta_1x+\beta_2y+\beta_3z-vt\right)\right)\end{array}\right]^{\frac{1}{2n}}\times\ e^{i(-\kappa_1x-\kappa_2y-\kappa_3z+\omega t+\zeta_0)}, \tag{34}$$

$$Q(x,y,z,t)=\left[\begin{array}{l}-\frac{(2n+1)c_2}{4(n+1)c_4}\pm\frac{1}{2(1+n)c_4}\sqrt{\frac{16(1+n)^3b_2c_4^2+\left(4n^3-3n-1\right)c_2^3}{2\left(1+m^2\right)(n-1)c_2}}\\ \times\mathrm{ns}\left(\frac{n}{(1+n)}\sqrt{-\frac{16(1+n)^3b_2c_4^2+\left(4n^3-3n-1\right)c_2^3}{2\left(m^2+1\right)(n-1)(2n+1)\Pi_1c_2c_4}}\left(\beta_1x+\beta_2y+\beta_3z-vt\right)\right)\end{array}\right]^{\frac{1}{2n}}\times\ e^{i(-\kappa_1x-\kappa_2y-\kappa_3z+\omega t+\zeta_0)}, \tag{35}$$

$$Q(x,y,z,t)=\left[\begin{array}{l}-\frac{(2n+1)c_2}{4(n+1)c_4}\pm\frac{m}{2(1+n)c_4}\sqrt{\frac{16(1+n)^3b_2c_4^2+\left(4n^3-3n-1\right)c_2^3}{2\left(1+m^2\right)(n-1)c_2}}\\ \times\mathrm{cd}\left(\frac{n}{(1+n)}\sqrt{-\frac{16(1+n)^3b_2c_4^2+\left(4n^3-3n-1\right)c_2^3}{2\left(m^2+1\right)(n-1)(2n+1)\Pi_1c_2c_4}}\left(\beta_1x+\beta_2y+\beta_3z-vt\right)\right)\end{array}\right]^{\frac{1}{2n}}\times\ e^{i(-\kappa_1x-\kappa_2y-\kappa_3z+\omega t+\zeta_0)}, \tag{36}$$

$$Q(x,y,z,t)=\left[\begin{array}{l}-\frac{(2n+1)c_2}{4(n+1)c_4}\pm\frac{1}{2(1+n)c_4}\sqrt{\frac{16(1+n)^3b_2c_4^2+\left(4n^3-3n-1\right)c_2^3}{2\left(1+m^2\right)(n-1)c_2}}\\ \times\,\mathrm{dc}\left(\frac{n}{(1+n)}\sqrt{-\frac{16(1+n)^3b_2c_4^2+\left(4n^3-3n-1\right)c_2^3}{2\left(m^2+1\right)(n-1)(2n+1)\Pi_1c_2c_4}}\left(\beta_1x+\beta_2y+\beta_3z-vt\right)\right)\end{array}\right]^{\frac{1}{2n}}\times\ e^{i(-\kappa_1x-\kappa_2y-\kappa_3z+\omega t+\zeta_0)},\tag{37}$$

provided that $c_2\left[16\ (1+n)^3\ b_2c_4^2+\left(4n^3-3n-1\right)c_2^3\right]>0$ and $\Pi_1c_4<0$.

When $m=1$ in Eqs (34) and (35), it leads to the optical domain wall solution and the singular soliton solution, respectively

$$Q(x,y,z,t)=\left[\begin{array}{l}-\frac{(2n+1)c_2}{4(1+n)c_4}\pm\frac{1}{4(1+n)c_4}\sqrt{\frac{16(1+n)^3b_2c_4^2+\left(4n^3-3n-1\right)c_2^3}{(n-1)c_2}}\\ \times\tanh\left(\frac{n}{2(1+n)}\sqrt{-\frac{16(1+n)^3b_2c_4^2+\left(4n^3-3n-1\right)c_2^3}{(n-1)(2n+1)\Pi_1c_2c_4}}\left(\beta_1x+\beta_2y+\beta_3z-vt\right)\right)\end{array}\right]^{\frac{1}{2n}}\times\ e^{i(-\kappa_1x-\kappa_2y-\kappa_3z+\omega t+\zeta_0)},\tag{38}$$

and

$$Q(x,y,z,t)=\left[\begin{array}{l}-\frac{(2n+1)c_2}{4(1+n)c_4}\pm\frac{1}{4(1+n)c_4}\sqrt{\frac{16(1+n)^3b_2c_4^2+\left(4n^3-3n-1\right)c_2^3}{(n-1)c_2}}\\ \times\coth\left(\frac{n}{2(1+n)}\sqrt{-\frac{16(1+n)^3b_2c_4^2+\left(4n^3-3n-1\right)c_2^3}{(n-1)(2n+1)\Pi_1c_2c_4}}\left(\beta_1x+\beta_2y+\beta_3z-vt\right)\right)\end{array}\right]^{\frac{1}{2n}}\times\ e^{i(-\kappa_1x-\kappa_2y-\kappa_3z+\omega t+\zeta_0)}.\tag{39}$$

Result 3. When setting $\chi_0=\dfrac{(1-m^2)\chi_2^2}{\left(2-m^2\right)^2\chi_4}$ in Eq (22) and solving it with Maple, the resulting solution remains the same as in Eq (23), along with the emergence of the following constraint conditions:

$$\left.\begin{array}{l}\omega=\dfrac{4\ (n+1)^2\,(n-1)\,(2n+1)\,\Pi_2c_2c_4+8\ (n+1)^3\,b_2c_4^2-\left(4n^3-3n-1\right)c_2^3}{4\,(n+1)^2\,(n-1)\,(2n+1)\,c_2c_4},\\ b_4=\dfrac{(2n-1)\left\{m^4(2n+1)^2(n-1)\left[32\,(n+1)^3b_2c_2^3c_4^2+(2n+1)^2(n-1)c_2^6\right]-1024\left(1-m^2\right)(n+1)^6b_2^2c_4^4\right\}}{256\left(2-m^2\right)^2(n-1)^2(n+1)^4(2n+1)c_2^2c_4^3}.\end{array}\right\}\tag{40}$$

By incorporating Eq (23) along with Eq (16) into Eq (21), it follows that Eq (1) presents the following solutions in accordance with the JEF:

$$Q(x,y,z,t)=\left[\begin{array}{l}-\frac{(2n+1)c_2}{4(1+n)c_4}\pm\frac{1}{2(1+n)c_4}\sqrt{\frac{16(1+n)^3b_2c_4^2+\left(4n^3-3n-1\right)c_2^3}{2\left(2-m^2\right)(n-1)c_2}}\\ \times\,\mathrm{dn}\left(\frac{n}{(1+n)}\sqrt{\frac{16(1+n)^3b_2c_4^2+\left(4n^3-3n-1\right)c_2^3}{2\left(2-m^2\right)(n-1)(2n+1)\Pi_1c_2c_4}}\left(\beta_1x+\beta_2y+\beta_3z-vt\right)\right)\end{array}\right]^{\frac{1}{2n}}\times\ e^{i(-\kappa_1x-\kappa_2y-\kappa_3z+\omega t+\zeta_0)},\tag{41}$$

provided that $c_2\left[16\ (1+n)^3 b_2 c_4^2 + \left(4n^3 - 3n - 1\right)c_2^3\right] > 0$ and $\Pi_1 c_4 > 0$.

$$Q(x,y,z,t) = \left[\begin{array}{l} -\frac{(2n+1)c_2}{4(1+n)c_4} \pm \frac{1}{2(1+n)c_4}\sqrt{\frac{\left(1-m^2\right)\left[16\,(1+n)^3 b_2 c_4^2+\left(4n^3-3n-1\right)c_2^3\right]}{2\left(2-m^2\right)(n-1)c_2}} \\ \times \mathrm{nd}\left(\frac{n}{(1+n)}\sqrt{\frac{16\,(1+n)^3 b_2 c_4^2+\left(4n^3-3n-1\right)c_2^3}{2\left(2-m^2\right)(n-1)(2n+1)\Pi_1 c_2 c_4}}\,(\beta_1 x+\beta_2 y+\beta_3 z-vt)\right) \end{array}\right]^{\frac{1}{2n}} \times\ e^{i(-\kappa_1 x-\kappa_2 y-\kappa_3 z+\omega t+\zeta_0)}, \tag{42}$$

provided that $c_2\left[16\ (1+n)^3 b_2 c_4^2 + \left(4n^3 - 3n - 1\right)c_2^3\right] > 0$ and $\Pi_1 c_4 > 0$.

$$Q(x,y,z,t) = \left[\begin{array}{l} -\frac{(2n+1)c_2}{4(1+n)c_4} \pm \frac{1}{2(1+n)c_4}\sqrt{-\frac{16\,(1+n)^3 b_2 c_4^2+\left(4n^3-3n-1\right)c_2^3}{2\left(2-m^2\right)(n-1)c_2}} \\ \times \mathrm{cs}\left(\frac{n}{(1+n)}\sqrt{\frac{16\,(1+n)^3 b_2 c_4^2+\left(4n^3-3n-1\right)c_2^3}{2\left(2-m^2\right)(n-1)(2n+1)\Pi_1 c_2 c_4}}\,(\beta_1 x+\beta_2 y+\beta_3 z-vt)\right) \end{array}\right]^{\frac{1}{2n}} \times\ e^{i(-\kappa_1 x-\kappa_2 y-\kappa_3 z+\omega t+\zeta_0)}, \tag{43}$$

provided that $c_2\left[16\ (1+n)^3 b_2 c_4^2 + \left(4n^3 - 3n - 1\right)c_2^3\right] < 0$ and $\Pi_1 c_4 < 0$.

$$Q(x,y,z,t) = \left[\begin{array}{l} -\frac{(2n+1)c_2}{4(1+n)c_4} \pm \frac{1}{2(1+n)c_4}\sqrt{-\frac{\left(1-m^2\right)\left[16\,(1+n)^3 b_2 c_4^2+\left(4n^3-3n-1\right)c_2^3\right]}{2\left(2-m^2\right)(n-1)c_2}} \\ \times \mathrm{sc}\left(\frac{n}{(1+n)}\sqrt{\frac{16\,(1+n)^3 b_2 c_4^2+\left(4n^3-3n-1\right)c_2^3}{2\left(2-m^2\right)(n-1)(2n+1)\Pi_1 c_2 c_4}}\,(\beta_1 x+\beta_2 y+\beta_3 z-vt)\right) \end{array}\right]^{\frac{1}{2n}} \times\ e^{i(-\kappa_1 x-\kappa_2 y-\kappa_3 z+\omega t+\zeta_0)}, \tag{44}$$

provided that $c_2\left[16\ (1+n)^3 b_2 c_4^2 + \left(4n^3 - 3n - 1\right)c_2^3\right] < 0$ and $\Pi_1 c_4 < 0$.

When $m = 0$ in Eqs (43) and (44), it leads to periodic solutions, respectively

$$Q(x,y,z,t) = \left[\begin{array}{l} -\frac{(2n+1)c_2}{4(1+n)c_4} \pm \frac{1}{4(1+n)c_4}\sqrt{-\frac{\left[16\,(1+n)^3 b_2 c_4^2+\left(4n^3-3n-1\right)c_2^3\right]}{(n-1)c_2}} \\ \times \cot\left(\frac{n}{2(1+n)}\sqrt{\frac{16\,(1+n)^3 b_2 c_4^2+\left(4n^3-3n-1\right)c_2^3}{(n-1)(2n+1)\Pi_1 c_2 c_4}}\,(\beta_1 x+\beta_2 y+\beta_3 z-vt)\right) \end{array}\right]^{\frac{1}{2n}} \times\ e^{i(-\kappa_1 x-\kappa_2 y-\kappa_3 z+\omega t+\zeta_0)}, \tag{45}$$

and

$$Q(x,y,z,t) = \left[\begin{array}{l} -\frac{(2n+1)c_2}{4(1+n)c_4} \pm \frac{1}{4(1+n)c_4}\sqrt{-\frac{\left[16\,(1+n)^3 b_2 c_4^2+\left(4n^3-3n-1\right)c_2^3\right]}{(n-1)c_2}} \\ \times \tan\left(\frac{n}{2(1+n)}\sqrt{\frac{16\,(1+n)^3 b_2 c_4^2+\left(4n^3-3n-1\right)c_2^3}{(n-1)(2n+1)\Pi_1 c_2 c_4}}\,(\beta_1 x+\beta_2 y+\beta_3 z-vt)\right) \end{array}\right]^{\frac{1}{2n}} \times\ e^{i(-\kappa_1 x-\kappa_2 y-\kappa_3 z+\omega t+\zeta_0)}. \tag{46}$$

Result 4. When setting $\chi_0 = \dfrac{(1-m^2)^2\chi_2^2}{4\left(1+m^2\right)^2\chi_4}$ in Eq (22) and solving it with Maple, the resulting solution remains the same as in Eq (23), along with the emergence of the following constraint conditions:

$$\left.\begin{aligned} \omega &= \frac{4\,(n+1)^2\,(n-1)\,(2n+1)\,\Pi_2 c_2 c_4 + 8\,(n+1)^3\,b_2 c_4^2 - \left(4n^3-3n-1\right)c_2^3}{4\,(n+1)^2\,(n-1)\,(2n+1)\,c_2 c_4}, \\ b_4 &= \frac{(2n-1)\left\{m^2(2n+1)^2(n-1)\left[32\,(n+1)^3 b_2 c_2^3 c_4^2 + (2n+1)^2(n-1)c_2^6\right] - 64\left(1-m^2\right)^2(n+1)^6 b_2^2 c_4^4\right\}}{64\left(1+m^2\right)^2(n-1)^2(n+1)^4(2n+1)c_2^2 c_4^3}. \end{aligned}\right\} \tag{47}$$

By incorporating Eq (23) along with Eq (17) into Eq (21), it follows that Eq (1) presents the following solutions in accordance with the JEF:

$$Q(x,y,z,t) = \left[-\frac{(2n+1)c_2}{4(1+n)c_4} \pm \frac{1}{4(1+n)c_4}\sqrt{\frac{16\,(1+n)^3 b_2 c_4^2 + \left(4n^3-3n-1\right)c_2^3}{\left(1+m^2\right)(n-1)c_2}} \times \left\{ \begin{array}{l} m\,\mathrm{cn}\left(\frac{n}{(1+n)}\sqrt{\frac{16\,(1+n)^3 b_2 c_4^2 + \left(4n^3-3n-1\right)c_2^3}{\left(1+m^2\right)(n-1)(2n+1)\Pi_1 c_2 c_4}}\,(\beta_1 x+\beta_2 y+\beta_3 z-vt)\right) \\ \\ \pm\mathrm{dn}\left(\frac{n}{(1+n)}\sqrt{\frac{16\,(1+n)^3 b_2 c_4^2 + \left(4n^3-3n-1\right)c_2^3}{\left(1+m^2\right)(n-1)(2n+1)\Pi_1 c_2 c_4}}\,(\beta_1 x+\beta_2 y+\beta_3 z-vt)\right) \end{array} \right\} \right]^{\frac{1}{2n}} \times\ e^{i(-\kappa_1 x-\kappa_2 y-\kappa_3 z+\omega t+\zeta_0)}, \tag{48}$$

provided that $c_2\left[16\,(1+n)^3\,b_2 c_4^2 + \left(4n^3-3n-1\right)c_2^3\right] > 0$ and $\Pi_1 c_4 > 0$.

$$Q(x,y,z,t) = \left[-\frac{(2n+1)c_2}{4(1+n)c_4} \pm \frac{1}{4(1+n)c_4}\sqrt{\frac{\left(1-m^2\right)\left[16\,(1+n)^3 b_2 c_4^2 + \left(4n^3-3n-1\right)c_2^3\right]}{\left(1+m^2\right)(n-1)c_2}} \times \left\{ \begin{array}{l} m\,\mathrm{sd}\left(\frac{n}{(1+n)}\sqrt{\frac{16\,(1+n)^3 b_2 c_4^2 + \left(4n^3-3n-1\right)c_2^3}{\left(1+m^2\right)(n-1)(2n+1)\Pi_1 c_2 c_4}}\,(\beta_1 x+\beta_2 y+\beta_3 z-vt)\right) \\ \\ \pm\mathrm{nd}\left(\frac{n}{(1+n)}\sqrt{\frac{16\,(1+n)^3 b_2 c_4^2 + \left(4n^3-3n-1\right)c_2^3}{\left(1+m^2\right)(n-1)(2n+1)\Pi_1 c_2 c_4}}\,(\beta_1 x+\beta_2 y+\beta_3 z-vt)\right) \end{array} \right\} \right]^{\frac{1}{2n}} \times\ e^{i(-\kappa_1 x-\kappa_2 y-\kappa_3 z+\omega t+\zeta_0)}, \tag{49}$$

provided that $c_2\left[16\,(1+n)^3\,b_2 c_4^2 + \left(4n^3-3n-1\right)c_2^3\right] > 0$ and $\Pi_1 c_4 > 0$.

$$Q(x,y,z,t) = \left[-\frac{(2n+1)c_2}{4(1+n)c_4} \pm \frac{1}{4(1+n)c_4}\sqrt{-\frac{\left(1-m^2\right)\left[16\,(1+n)^3 b_2 c_4^2 + \left(4n^3-3n-1\right)c_2^3\right]}{\left(1+m^2\right)(n-1)c_2}} \times \left\{ \begin{array}{l} \mathrm{nc}\left(\frac{n}{(1+n)}\sqrt{\frac{16\,(1+n)^3 b_2 c_4^2 + \left(4n^3-3n-1\right)c_2^3}{\left(1+m^2\right)(n-1)(2n+1)\Pi_1 c_2 c_4}}\,(\beta_1 x+\beta_2 y+\beta_3 z-vt)\right) \\ \\ \pm\mathrm{sc}\left(\frac{n}{(1+n)}\sqrt{\frac{16\,(1+n)^3 b_2 c_4^2 + \left(4n^3-3n-1\right)c_2^3}{\left(1+m^2\right)(n-1)(2n+1)\Pi_1 c_2 c_4}}\,(\beta_1 x+\beta_2 y+\beta_3 z-vt)\right) \end{array} \right\} \right]^{\frac{1}{2n}} \times\ e^{i(-\kappa_1 x-\kappa_2 y-\kappa_3 z+\omega t+\zeta_0)}, \tag{50}$$

provided that $c_2\left[16\ (1+n)^3 b_2 c_4^2+\left(4n^3-3n-1\right)c_2^3\right]<0$ and $\Pi_1 c_4<0$.

$$Q(x,y,z,t)=\left[\begin{array}{l}-\frac{(2n+1)c_2}{4(1+n)c_4}\pm\frac{1}{4(1+n)c_4}\sqrt{-\frac{\left(1-m^2\right)\left[16\,(1+n)^3 b_2c_4^2+\left(4n^3-3n-1\right)c_2^3\right]}{\left(1+m^2\right)(n-1)c_2}}\\ \times\left\{\frac{\mathrm{cn}\left(\frac{n}{(1+n)}\sqrt{\frac{16\,(1+n)^3 b_2c_4^2+\left(4n^3-3n-1\right)c_2^3}{\left(1+m^2\right)(n-1)(2n+1)\Pi_1 c_2c_4}}\,(\beta_1x+\beta_2y+\beta_3z-vt)\right)}{1\pm\mathrm{sn}\left(\frac{n}{(1+n)}\sqrt{\frac{16\,(1+n)^3 b_2c_4^2+\left(4n^3-3n-1\right)c_2^3}{\left(1+m^2\right)(n-1)(2n+1)\Pi_1 c_2c_4}}\,(\beta_1x+\beta_2y+\beta_3z-vt)\right)}\right\}\end{array}\right]^{\frac{1}{2n}}\times\ e^{i(-\kappa_1x-\kappa_2y-\kappa_3z+\omega t+\zeta_0)},\tag{51}$$

provided that $c_2\left[16\ (1+n)^3 b_2c_4^2+\left(4n^3-3n-1\right)c_2^3\right]<0$ and $\Pi_1 c_4<0$.

When $m=0$ in Eqs (50) and (51), it results in the periodic solutions, respectively:

$$Q(x,y,z,t)=\left[\begin{array}{l}-\frac{(2n+1)c_2}{4(1+n)c_4}\pm\frac{1}{4(1+n)c_4}\sqrt{-\frac{\left[16\,(1+n)^3 b_2c_4^2+\left(4n^3-3n-1\right)c_2^3\right]}{2(n-1)c_2}}\\ \times\left\{\begin{array}{l}\sec\left(\frac{n}{(1+n)}\sqrt{\frac{16\,(1+n)^3 b_2c_4^2+\left(4n^3-3n-1\right)c_2^3}{2(n-1)(2n+1)\Pi_1 c_2c_4}}\,(\beta_1x+\beta_2y+\beta_3z-vt)\right)\\ \pm\tan\left(\frac{n}{(1+n)}\sqrt{\frac{16\,(1+n)^3 b_2c_4^2+\left(4n^3-3n-1\right)c_2^3}{2(n-1)(2n+1)\Pi_1 c_2c_4}}\,(\beta_1x+\beta_2y+\beta_3z-vt)\right)\end{array}\right\}\end{array}\right]^{\frac{1}{2n}}\times\ e^{i(-\kappa_1x-\kappa_2y-\kappa_3z+\omega t+\zeta_0)},\tag{52}$$

and

$$Q(x,y,z,t)=\left[\begin{array}{l}-\frac{(2n+1)c_2}{4(1+n)c_4}\pm\frac{1}{4(1+n)c_4}\sqrt{-\frac{\left[16\,(1+n)^3 b_2c_4^2+\left(4n^3-3n-1\right)c_2^3\right]}{(n-1)c_2}}\\ \times\left\{\frac{\cos\left(\frac{n}{(1+n)}\sqrt{\frac{16\,(1+n)^3 b_2c_4^2+\left(4n^3-3n-1\right)c_2^3}{(n-1)(2n+1)\Pi_1 c_2c_4}}\,(\beta_1x+\beta_2y+\beta_3z-vt)\right)}{1\pm\sin\left(\frac{n}{(1+n)}\sqrt{\frac{16\,(1+n)^3 b_2c_4^2+\left(4n^3-3n-1\right)c_2^3}{(n-1)(2n+1)\Pi_1 c_2c_4}}\,(\beta_1x+\beta_2y+\beta_3z-vt)\right)}\right\}\end{array}\right]^{\frac{1}{2n}}\times\ e^{i(-\kappa_1x-\kappa_2y-\kappa_3z+\omega t+\zeta_0)}.\tag{53}$$

Result 5. When setting $\chi_0=\dfrac{m^4\chi_2^2}{4\left(2-m^2\right)^2\chi_4}$ in Eq (22) and solving it with Maple, the resulting solution remains the same as in Eq (23), along with the emergence of the following constraint conditions:

$$\left.\begin{array}{l}\omega=\dfrac{4\ (n+1)^2(n-1)(2n+1)\Pi_2c_2c_4+8\ (n+1)^3 b_2c_4^2-\left(4n^3-3n-1\right)c_2^3}{4\,(n+1)^2(n-1)(2n+1)c_2c_4},\\ b_4=\dfrac{(2n-1)\left\{\left(1-m^2\right)(2n+1)^2(n-1)\left[32\,(n+1)^3b_2c_2^3c_4^2+(2n+1)^2(n-1)c_2^6\right]-64m^4(n+1)^6b_2^2c_4^4\right\}}{64\left(2-m^2\right)^2(n-1)^2(n+1)^4(2n+1)c_2^2c_4^3}.\end{array}\right\}\tag{54}$$

By incorporating Eq (23) along with Eq (18) into Eq (21), it follows that Eq (1) presents the following solutions in accordance with the JEF:

$$Q(x,y,z,t)=\left[\begin{array}{l} -\frac{(2n+1)c_2}{4(1+n)c_4}\pm\frac{1}{4(1+n)c_4}\sqrt{\frac{16(1+n)^3b_2c_4^2+\left(4n^3-3n-1\right)c_2^3}{\left(2-m^2\right)(n-1)c_2}} \\ \times\left\{\begin{array}{l} \sqrt{1-m^2}\,\mathrm{nc}\left(\frac{n}{(1+n)}\sqrt{-\frac{16(1+n)^3b_2c_4^2+\left(4n^3-3n-1\right)c_2^3}{\left(2-m^2\right)(n-1)(2n+1)\Pi_1c_2c_4}}\left(\beta_1x+\beta_2y+\beta_3z-vt\right)\right) \\ \pm\mathrm{dc}\left(\frac{n}{(1+n)}\sqrt{-\frac{16(1+n)^3b_2c_4^2+\left(4n^3-3n-1\right)c_2^3}{\left(2-m^2\right)(n-1)(2n+1)\Pi_1c_2c_4}}\left(\beta_1x+\beta_2y+\beta_3z-vt\right)\right) \end{array}\right\} \end{array}\right]^{\frac{1}{2n}} \times\ e^{i(-\kappa_1x-\kappa_2y-\kappa_3z+\omega t+\zeta_0)}, \tag{55}$$

provided that $c_2\left[16\ (1+n)^3\,b_2c_4^2+\left(4n^3-3n-1\right)c_2^3\right]>0$ and $\Pi_1c_4<0$.

Result 6. Solving (22) with Maple reveals the following results:

$$\gamma_0=-\frac{c_2\,(2n+1)}{4c_4\,(n+1)},\ \gamma_0=\pm\tfrac{1}{2n}\sqrt{-\frac{(2n+1)\,\Pi_1\chi_4}{c_4}},\ \chi_2=\frac{\left[16\ (n+1)^3\,b_2c_4^2+\left(4n^3-3n-1\right)c_2^3\right]n^2}{2\,(n+1)^2\,(n-1)\,(2n+1)\,\Pi_1c_2c_4},$$

$$\chi_0=\frac{[32\ (n+1)^3\left(4n^2-1\right)b_2c_2c_4^2-256\,b_4c_4^3\,(n-1)\,(n+1)^4+\left(4n^2-1\right)(2n+1)^2\,(n-1)\,c_2^4]n^4}{16\,(4n^2-1)\,(n+1)^4\,(n-1)\,\Pi_1^2\chi_4c_4^2}, \tag{56}$$

and

$$\omega=\frac{4\ (n+1)^2\,(n-1)\,(2n+1)\,\Pi_2c_2c_4+8\ (n+1)^3\,b_2c_4^2-\left(4n^3-3n-1\right)c_2^3}{4\,(n+1)^2\,(n-1)\,(2n+1)\,c_2c_4}, \tag{57}$$

assuming that $\Pi_1\chi 4c4<0$. By integrating Eq (56) along with Eq (19) into Eq (21), it follows that Eq (1) has the following solutions expressed in terms of WEFs

$$Q(x,y,z,t)=\left[\begin{array}{l} -\frac{(2n+1)c_2}{4(1+n)c_4}\pm\frac{1}{2n}\sqrt{-\frac{(2n+1)\,\Pi_1}{c_4}} \\ \times\frac{3\wp'\left(\beta_1x+\beta_2y+\beta_3z-vt,l_2,l_3\right)}{\left\{6\wp\left(\beta_1x+\beta_2y+\beta_3z-vt,l_2,l_3\right)+\frac{\left[16\ (n+1)^3\,b_2c_4^2+\left(4n^3-3n-1\right)c_2^3\right]n^2}{2\,(n+1)^2\,(n-1)\,(2n+1)\,\Pi_1c_2c_4}\right\}} \end{array}\right]^{\frac{1}{2n}} \times\ e^{i(-\kappa_1x-\kappa_2y-\kappa_3z+\omega t+\zeta_0)}, \tag{58}$$

and

$$Q(x,y,z,t)=\left[\begin{array}{l}-\frac{(2n+1)c_2}{4(1+n)c_4}\pm\frac{1}{2n}\sqrt{-\frac{(2n+1)\Pi_1}{c_4}}\\ \times\sqrt{\frac{[32(n+1)^3\left(4n^2-1\right)b_2c_2c_4^2-256b_4c_4^3(n-1)(n+1)^4+\left(4n^2-1\right)(2n+1)^2(n-1)c_2^4]n^4}{16\left(4n^2-1\right)(n+1)^4(n-1)\Pi_1^2c_4^2}}\\ \times\frac{12(n+1)^2(n-1)(2n+1)\Pi_1c_2c_4\wp(\beta_1x+\beta_2y+\beta_3z-vt,l_2,l_3)+16n^2(n+1)^3b_2c_4^2+n^2\left(4n^3-3n-1\right)c_2^3}{6(n+1)^2(n-1)(2n+1)\Pi_1c_2c_4\wp'(\beta_1x+\beta_2y+\beta_3z-vt,l_2,l_3)}\end{array}\right]^{\frac{1}{2n}}\times e^{i(-\kappa_1x-\kappa_2y-\kappa_3z+\omega t+\zeta_0)},\tag{59}$$

where

$$l_2=\frac{\left\{n^4(2n-1)\left[c_2^6(n-1)^2(2n+1)^4+32(n-1)(n+1)^3(2n+1)^2c_4^2c_2^3b_2+64(n+1)^6b_2^2c_4^4\right]-192n^4c_4^3c_2^2b_4(n-1)^2(n+1)^4(2n+1)\right\}}{12c_2^2c_4^2\Pi_1^2(n-1)^2(n+1)^4(2n-1)(2n+1)^2},$$

$$\begin{aligned}l_3=&\frac{1}{216(2n-1)(2n+1)^3(n+1)^6c_2^3\Pi_1^3c_4^3(n-1)^3}\left\{-288n^6(2n+1)^3(n-1)^3(n+1)^4b_4c_4^3c_2^5\right.\\&+32n^6\left[15(2n+1)^2(n-1)b_2^2c_4^4c_2^3-16(n+1)^3b_2^3c_4^6\right](2n-1)(n+1)^6\\&-4608n^6(n+1)^7(n-1)^2(2n+1)b_2b_4c_2^2c_4^5\\&\left.+\left[48n^6(n+1)^3b_2c_4^2c_2^6+n^6(n-1)(2n+1)^2c_2^9\right](2n-1)(n-1)^2(2n+1)^4\right\},\end{aligned}\tag{60}$$

provided that $\left(2m^2-1\right)c_2\left[16(1+n)^3b_2c_4^2+\left(4n^3-3n-1\right)c_2^3\right]>0$ and $\Pi_1c_4>0$.

5. Results and discussion

This section provides an in-depth analysis of the soliton's behavior and characteristics depicted in Figures 1–15. The figures illustrate various soliton solutions, including bright solitons, singular solitons, dark solitons, and periodic solutions, using the time parameter $t = 1$ and the power nonlinearity parameters $n = 1, 2$, and 3. Each set of figures addresses different aspects of the soliton solutions, including their modulus, real part, and imaginary part, presented through surface plots, contour plots, and two-dimensional (2D) plots. The parameters used in Figures 1–15 are: $\beta_1 = 0.15$, $\beta_2 = 0$, $\beta_3 = 0$, $a_1 = 0.2$, $a_2 = 0.3$, $a_3 = 0.35$, $a_4 = 0.4$, $a_5 = -0.45$, $a_6 = -0.5$, $\kappa_1 = 0.18$, $\kappa_2 = 0$, $\kappa_3 = 0$, $b_2 = 0.31$, $b_4 = 0.4$, $n = 1$, $n = 2$, $n = 3$, $\omega = 0.55$, $v = 0.3$, and $\zeta_0 = 0$.

Figures 1–3 explore the characteristics of the bright soliton described by the complex-valued solution (29). These figures present the soliton's modulus, real part, and imaginary part, as influenced by the power nonlinearity parameters $n = 1$, $n = 2$, and $n = 3$. For $n = 1$ in Figure 1, the surface plots in Figure 1(a), (d), and (g) reveal a highly localized bright soliton with a pronounced peak in its modulus, suggesting strong confinement of energy in space. The contour plots in Figure 1(b), (e), and (h) exhibit circular symmetry, indicating that the soliton maintains its shape during its evolution. The 2D plots in Figure 1(c), (f), and (i) confirm the stability of the soliton under these conditions, with

minimal deformation as it propagates through space. In Figure 2, increasing the nonlinearity parameter to $n = 2$ results in a broader soliton profile, as shown in the surface plots (Figure 2(a), (d), and (g)). The energy spreads more widely compared with $n = 1$, and the contour plots (Figure 2(b), (e), and (h)) show less pronounced symmetry. The 2D plots (Figure 2(c), (f), and (i)) demonstrate that while the soliton remains stable, it experiences minor broadening, indicating a stronger influence of nonlinearity. When the nonlinearity parameter increases to $n = 3$ (Figure 3), the soliton becomes even broader, as evidenced by the surface plots (Figure 3(a), (d), and (g)). The contour plots (Figure 3(b), (e), and (h)) show further weakening of the central peak, and the 2D plots (Figure 3(c), (f), and (i)) reveal a more diffuse structure. This suggests that higher-power nonlinearity induces a significant broadening effect, making the bright soliton less confined in space.

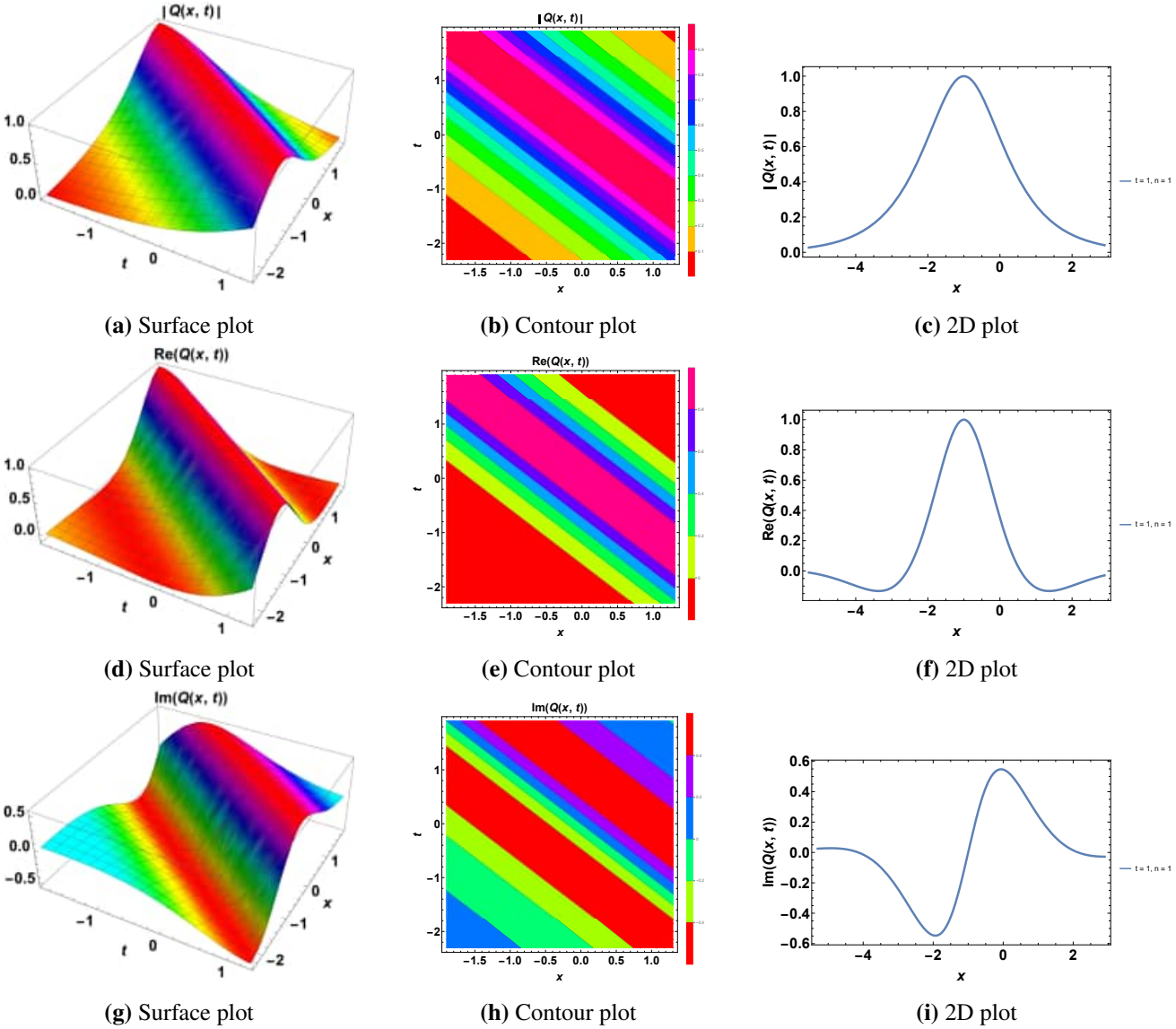

(a) Surface plot **(b)** Contour plot **(c)** 2D plot

(d) Surface plot **(e)** Contour plot **(f)** 2D plot

(g) Surface plot **(h)** Contour plot **(i)** 2D plot

Figure 1. Profile of a bright soliton given $n = 1$.

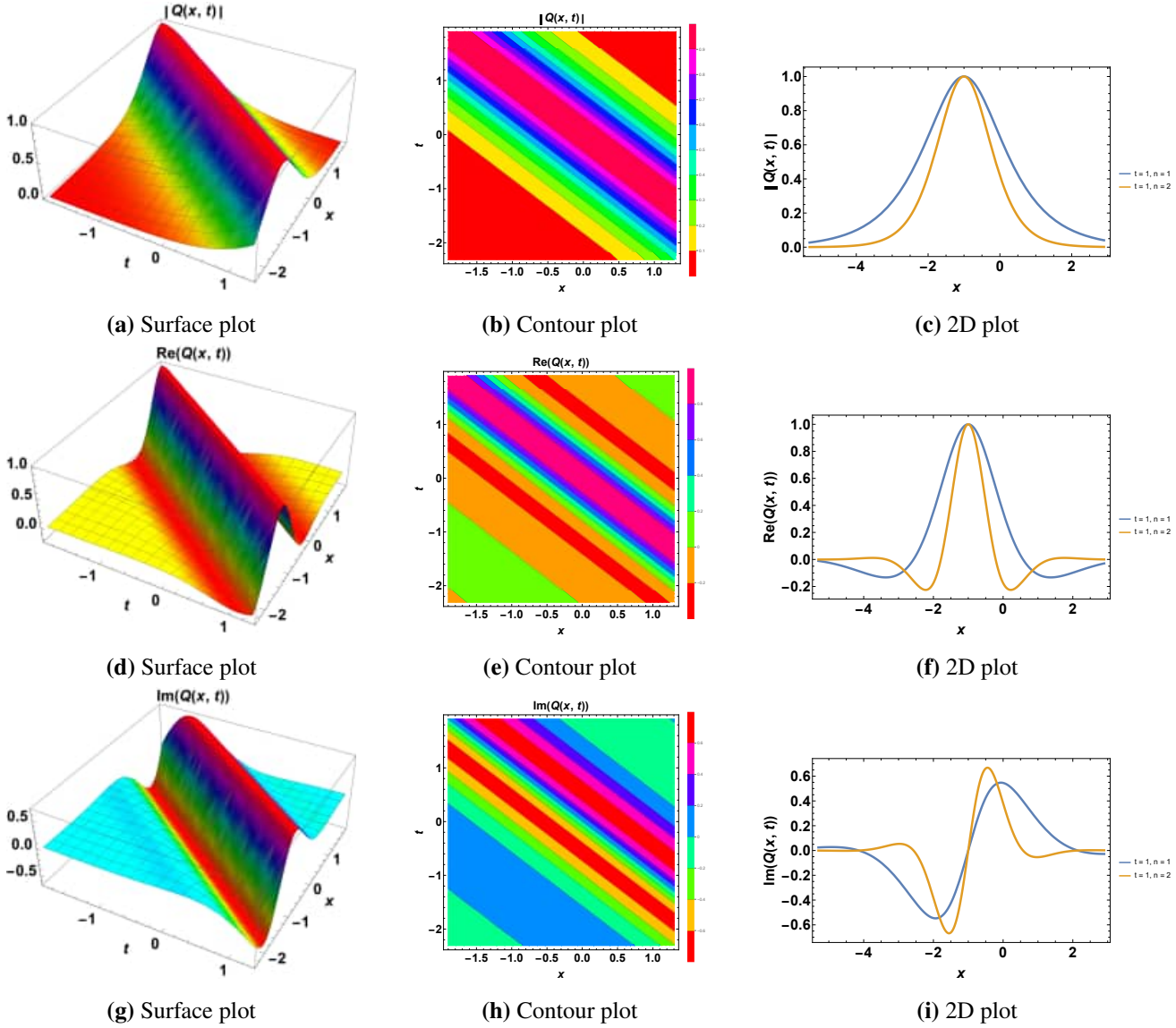

(a) Surface plot **(b)** Contour plot **(c)** 2D plot

(d) Surface plot **(e)** Contour plot **(f)** 2D plot

(g) Surface plot **(h)** Contour plot **(i)** 2D plot

Figure 2. Profile of a bright soliton given $n = 2$.

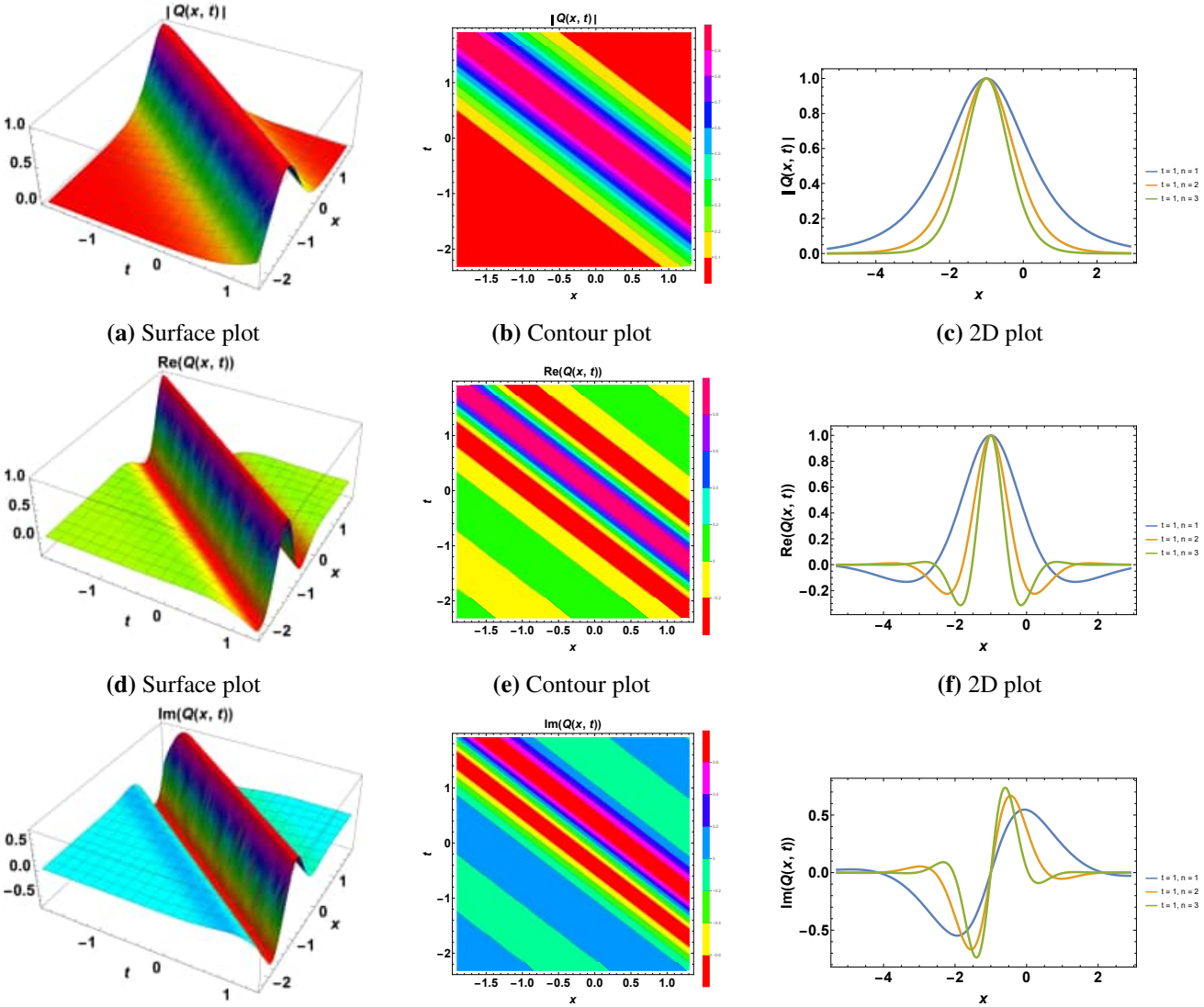

(a) Surface plot **(b)** Contour plot **(c)** 2D plot

(d) Surface plot **(e)** Contour plot **(f)** 2D plot

(g) Surface plot **(h)** Contour plot **(i)** 2D plot

Figure 3. Profile of a bright soliton given $n = 3$.

Figures 4–6 illustrate the singular soliton's behavior using the complex-valued solution (30), again for $n = 1$, $n = 2$, and $n = 3$. Singular solitons are known for their sharp, divergent profiles, and the figures reveal how these profiles evolve under different nonlinearity conditions. For $n = 1$ in Figure 4, the surface plots (Figure 4(a), (d), and (g)) highlight the sharply peaked and highly localized nature of the singular soliton for $n = 1$. The soliton's modulus exhibits a singularity at the core, with the real and imaginary parts showing steep gradients near this point. The contour plots (Figure 4(b), (e), and (h)) clearly indicate the divergence at the center, and the 2D plots (Figure 4(c), (f), and (i)) show the steepness of the soliton, typical of singular solutions. As the nonlinearity increases to $n = 2$ in Figure 5, the singularity becomes more pronounced, as seen in the surface plots (Figure 5(a), (d), and (g)). The contour plots (Figures 5(b), (e), and (h)) show that the energy distribution remains tightly confined to the singularity, and the 2D plots (Figure 5(c), (f), and (i)) reveal a sharper peak than in Figure 4, demonstrating the enhanced focusing effect of increased nonlinearity. Figure 6 shows that for $n = 3$,

the singularity reaches an extreme, with the surface plots (Figure 6(a), (d), and (g)) displaying a very narrow and highly localized peak. The contour plots (Figure 6(b), (e), and (h)) confirm the intense confinement of energy around the singularity, while the 2D plots (Figure 6(c), (f), and (i)) depict a highly steep and sharp structure, characteristic of singular solitons under strong nonlinearity.

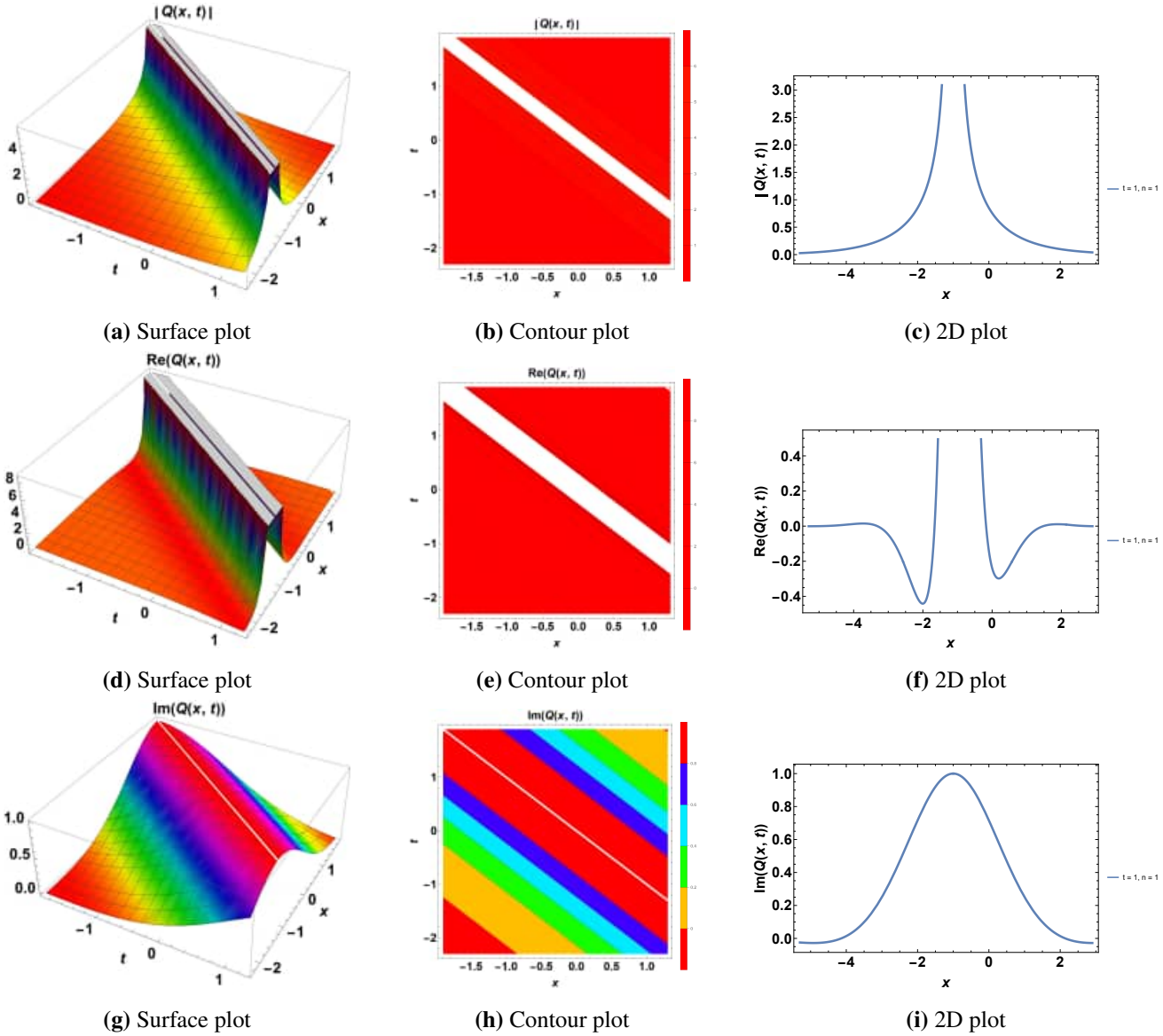

(a) Surface plot **(b)** Contour plot **(c)** 2D plot

(d) Surface plot **(e)** Contour plot **(f)** 2D plot

(g) Surface plot **(h)** Contour plot **(i)** 2D plot

Figure 4. Profile of a singular soliton given $n = 1$.

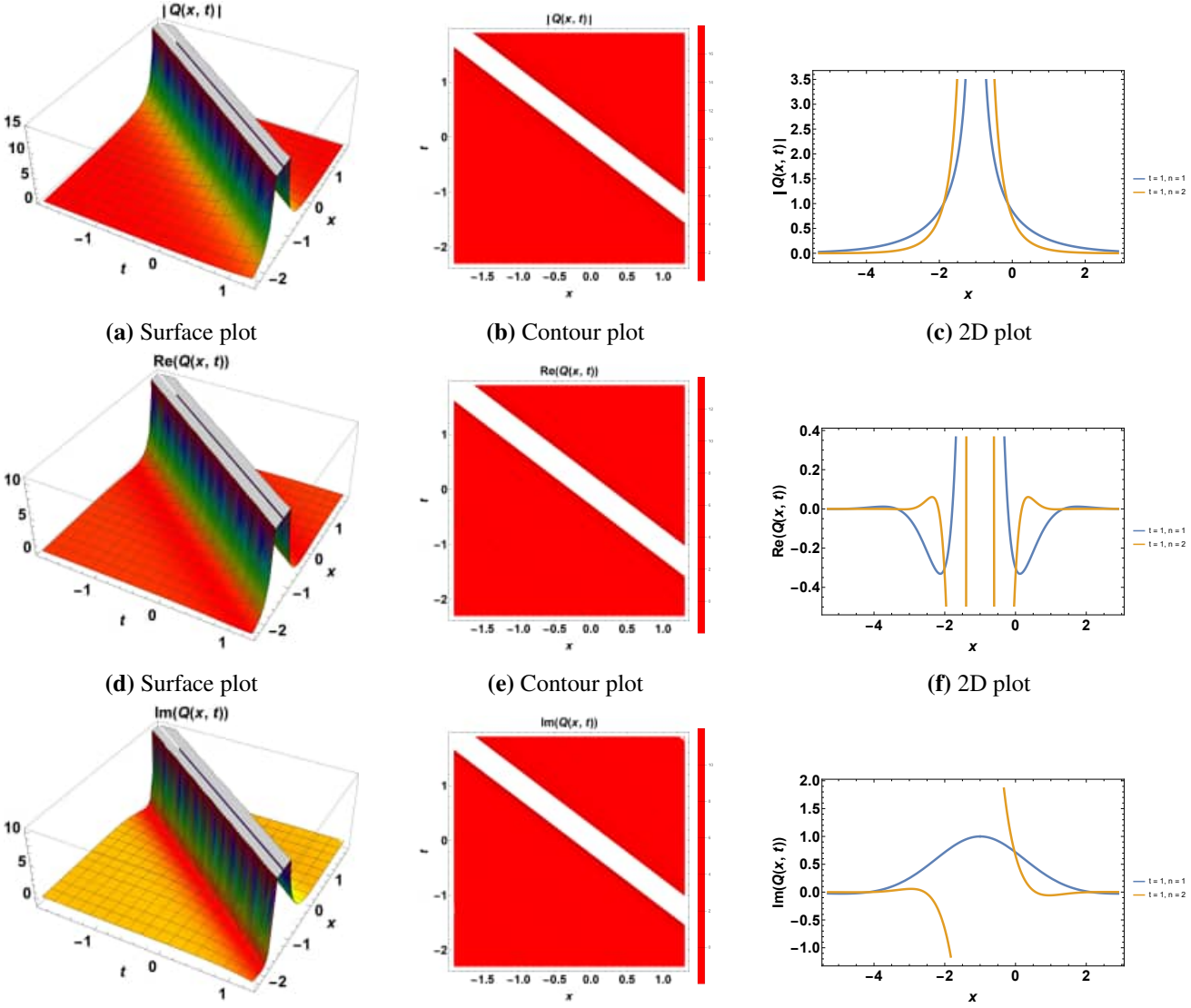

(a) Surface plot **(b)** Contour plot **(c)** 2D plot

(d) Surface plot **(e)** Contour plot **(f)** 2D plot

(g) Surface plot **(h)** Contour plot **(i)** 2D plot

Figure 5. Profile of a singular soliton given $n = 2$.

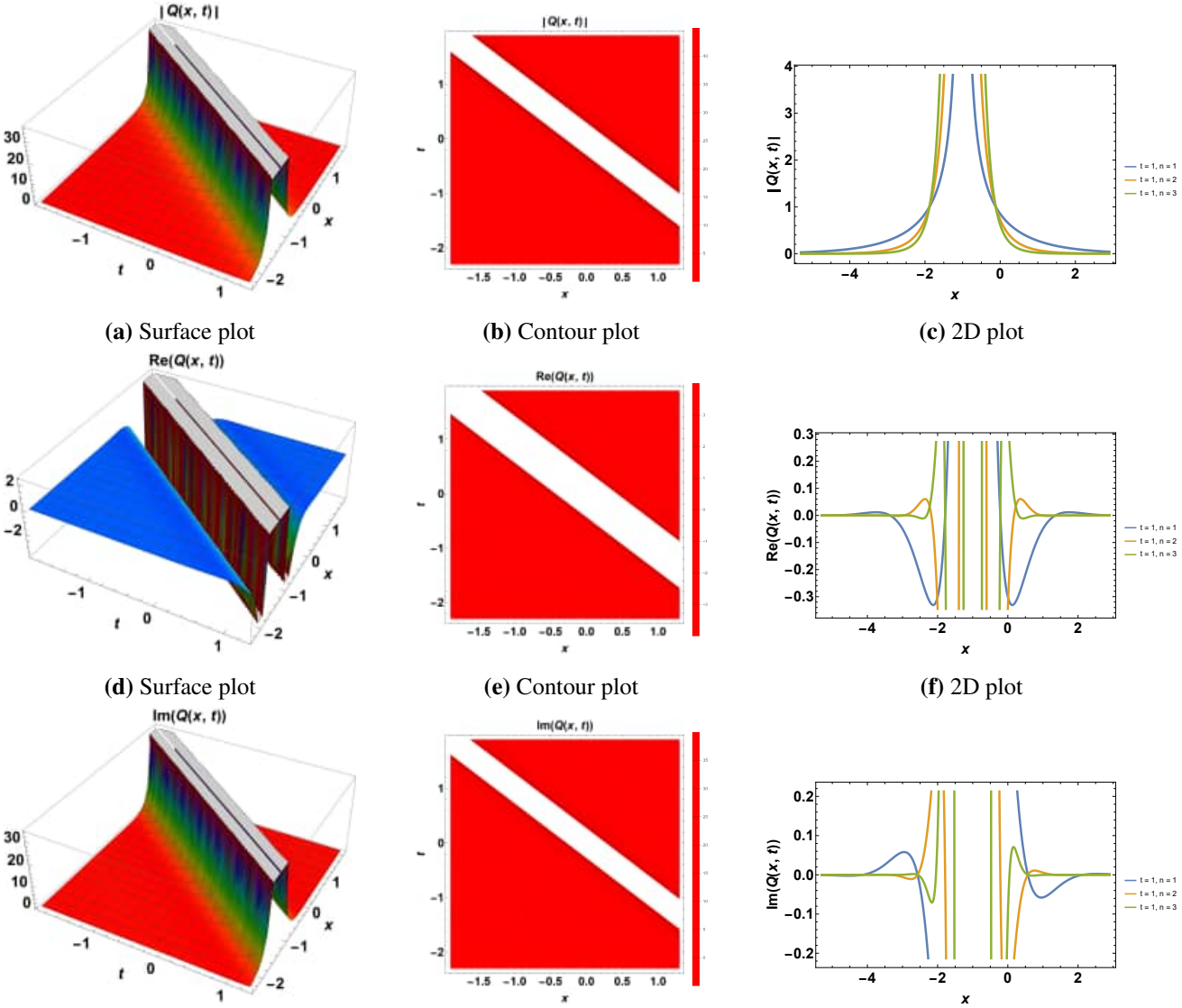

(a) Surface plot **(b)** Contour plot **(c)** 2D plot

(d) Surface plot **(e)** Contour plot **(f)** 2D plot

(g) Surface plot **(h)** Contour plot **(i)** 2D plot

Figure 6. Profile of a singular soliton given $n = 3$.

Figures 7–9 analyze the evolution of dark solitons, which are described by the complex-valued solution (38). Dark solitons are characterized by a dip in their modulus, surrounded by a flat background. For $n = 1$ in Figure 7, the dark soliton exhibits a pronounced dip in its modulus, as shown in the surface plots (Figure 7(a), (d), and (g)). The real part displays an antisymmetric structure, while the imaginary part shows a flat profile. The contour plots (Figure 7(b), (e), and (h)) demonstrate that the dark soliton maintains a flat background, and the 2D plots (Figure 7(c), (f), and (i)) highlight the clear dip in the modulus at the soliton's center. Increasing n to 2 results in a more pronounced dip, as illustrated in Figure 8. The surface plots (Figure 8(a), (d), and (g)) show a deeper trough in the modulus, and the contour plots (Figure 8(b), (e), and (h)) depict a sharper contrast between the soliton's center and the surrounding background. The 2D plots (Figure 8(c), (f), and (i)) reveal that the dip becomes more pronounced, indicating the influence of stronger nonlinearity. With $n = 3$ (Figure 9), the dark soliton's dip becomes even deeper, as seen in the surface plots (Figure 9(a),

(d), and (g)). The contour plots (Figure 9(b), (e), and (h)) show a well-defined trough, and the 2D plots (Figure 9(c), (f), and (i)) reveal that the dark soliton becomes more pronounced with increasing nonlinearity, indicating the strong influence of the power nonlinearity parameter on the soliton's shape.

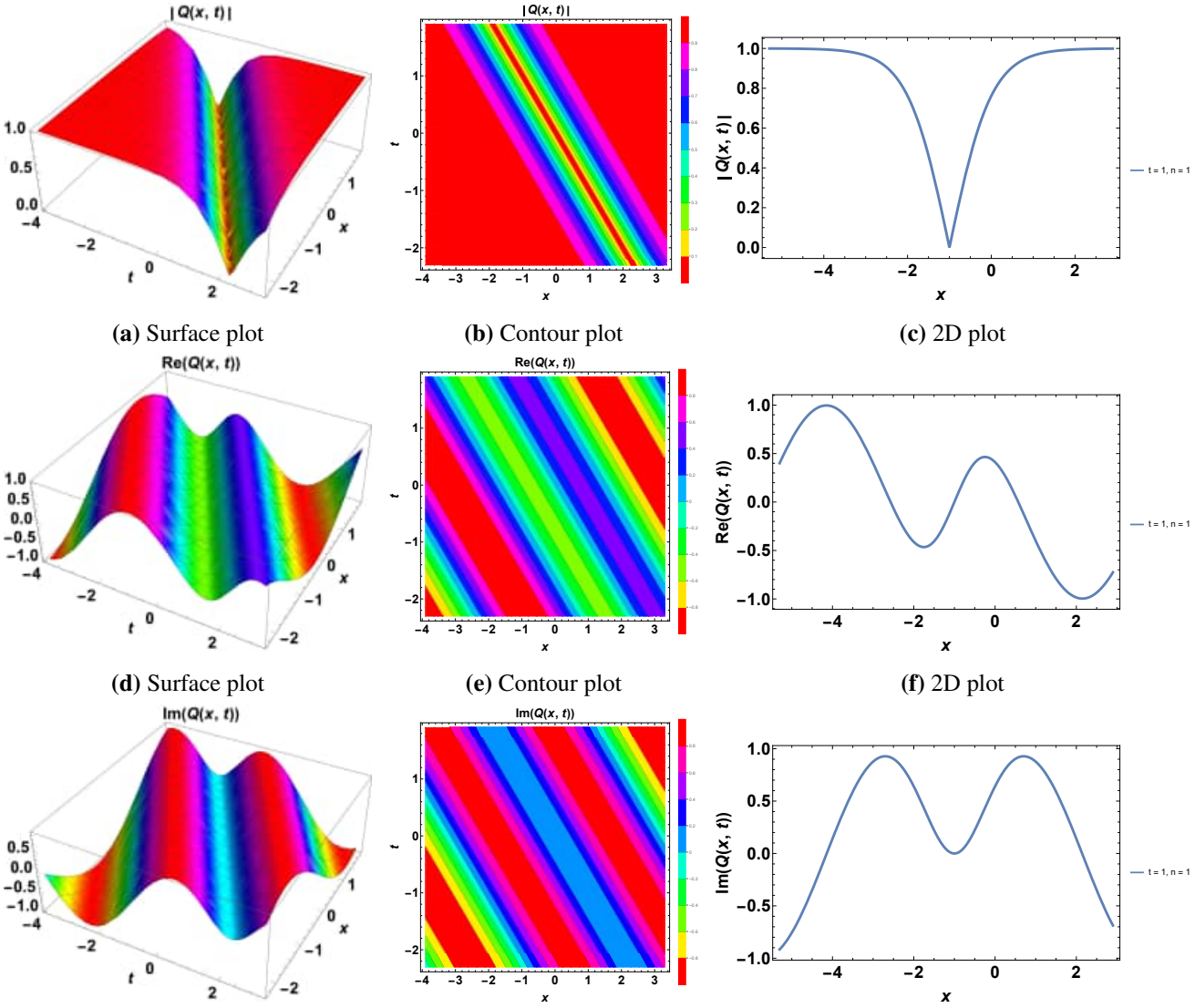

(a) Surface plot **(b)** Contour plot **(c)** 2D plot

(d) Surface plot **(e)** Contour plot **(f)** 2D plot

(g) Surface plot **(h)** Contour plot **(i)** 2D plot

Figure 7. Profile of a dark soliton given $n = 1$.

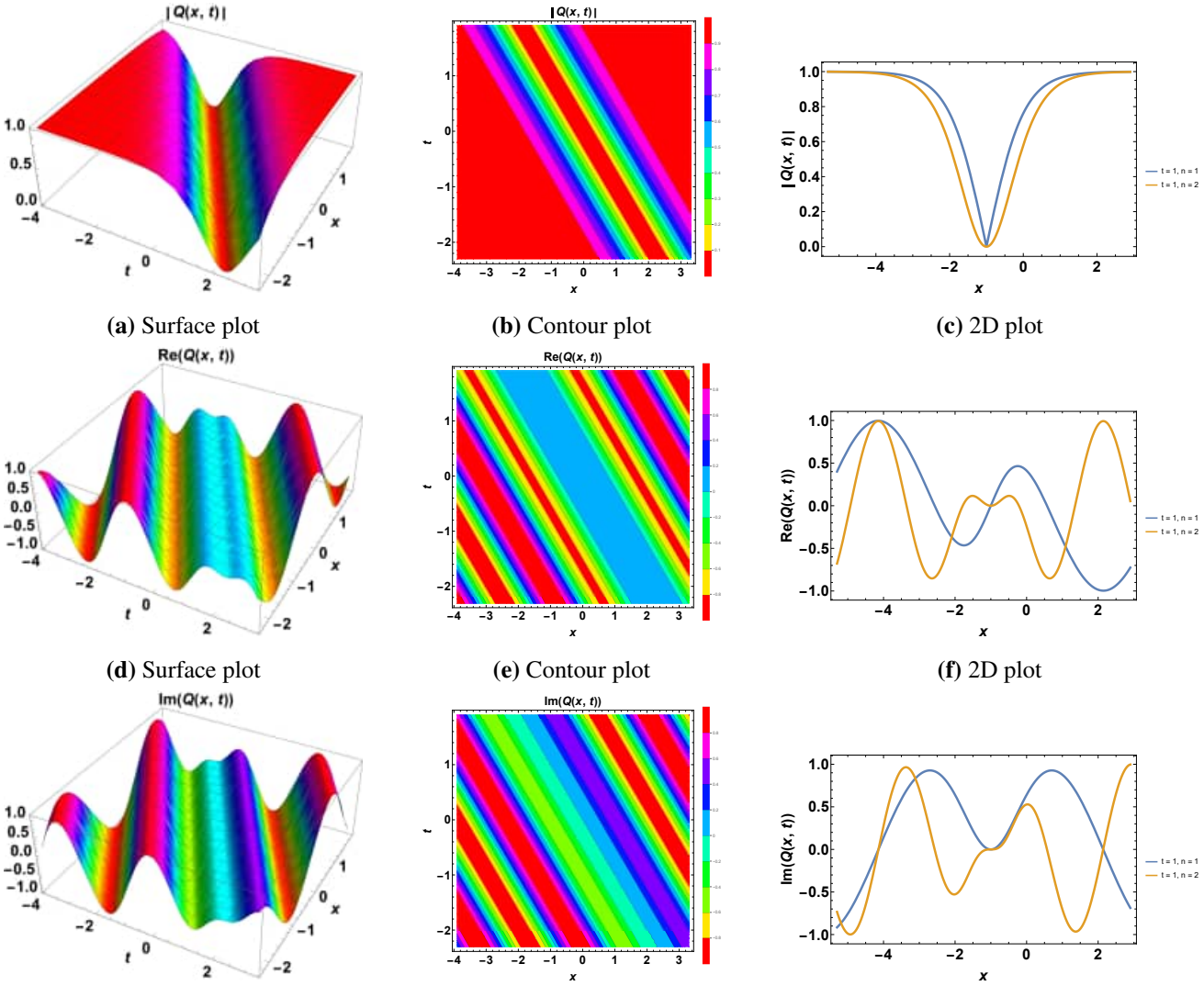

(a) Surface plot **(b)** Contour plot **(c)** 2D plot

(d) Surface plot **(e)** Contour plot **(f)** 2D plot

(g) Surface plot **(h)** Contour plot **(i)** 2D plot

Figure 8. Profile of a dark soliton given $n = 2$.

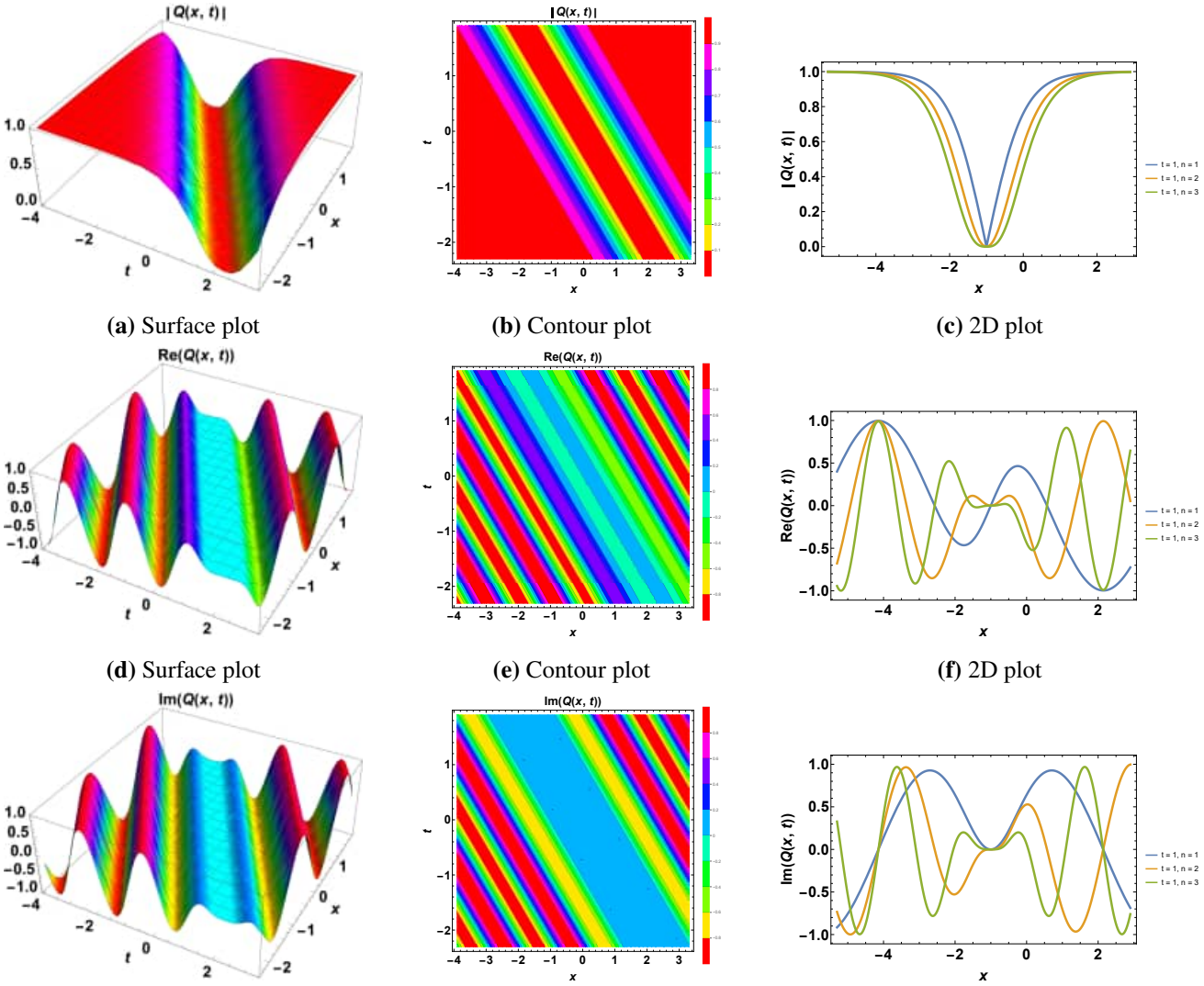

(a) Surface plot **(b)** Contour plot **(c)** 2D plot

(d) Surface plot **(e)** Contour plot **(f)** 2D plot

(g) Surface plot **(h)** Contour plot **(i)** 2D plot

Figure 9. Profile of a dark soliton given $n = 3$.

Figures 10–12 present another set of singular soliton solutions using the complex-valued solution (39). The characteristics of these solitons are similar to those in Figures 4–6, with the key difference being the specific form of the solution. For $n = 1$ in Figure 10, the singularity is prominent, as shown in the surface plots (Figure 10(a), (d), and (g)). The contour plots (Figure 10(b), (e), and (h)) indicate the sharp peak characteristic of singular solitons, and the 2D plots (Figure 10(c), (f), and (i)) show the steep gradient near the singularity. Figure 11 illustrates that for $n = 2$, the singularity becomes sharper, as seen in the surface plots (Figure 11(a), (d), and (g)). The contour plots (Figure 11(b), (e), and (h)) show a more localized energy concentration, and the 2D plots (Figure 11(c), (f), and (i)) depict an increasingly steep gradient at the singularity's core. In Figure 12, for $n = 3$, the singularity becomes extremely sharp and localized, as evidenced by the surface plots (Figure 12(a), (d), and (g)), contour plots (Figure 12(b), (e), and (h)), and 2D plots (Figure 12(c), (f), and (i)). The soliton's peak sharpens significantly, illustrating the strong focusing effect of high-power nonlinearity.

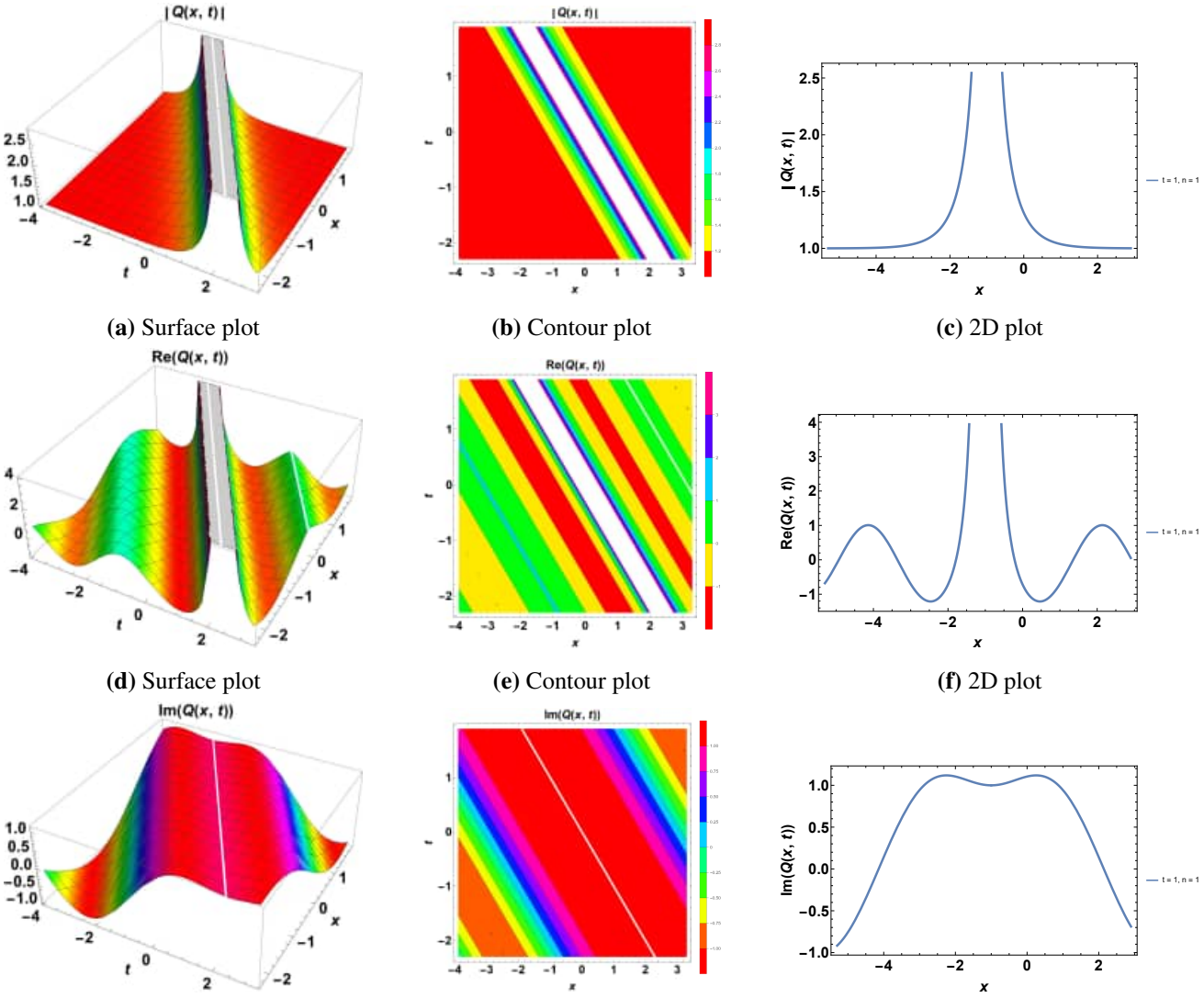

(a) Surface plot **(b)** Contour plot **(c)** 2D plot

(d) Surface plot **(e)** Contour plot **(f)** 2D plot

(g) Surface plot **(h)** Contour plot **(i)** 2D plot

Figure 10. Profile of a singular soliton given $n = 1$.

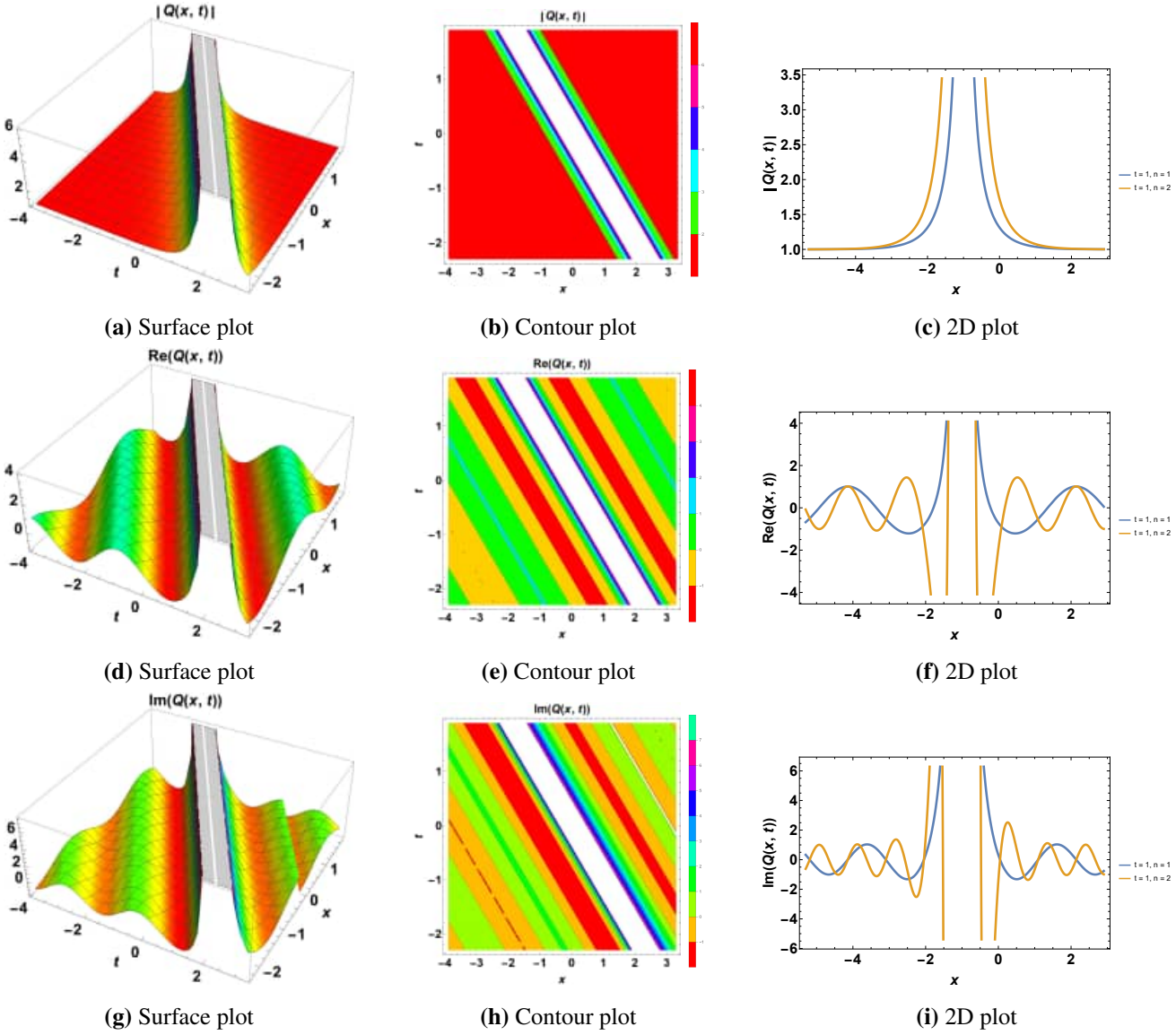

(a) Surface plot **(b)** Contour plot **(c)** 2D plot

(d) Surface plot **(e)** Contour plot **(f)** 2D plot

(g) Surface plot **(h)** Contour plot **(i)** 2D plot

Figure 11. Profile of a singular soliton given $n = 2$.

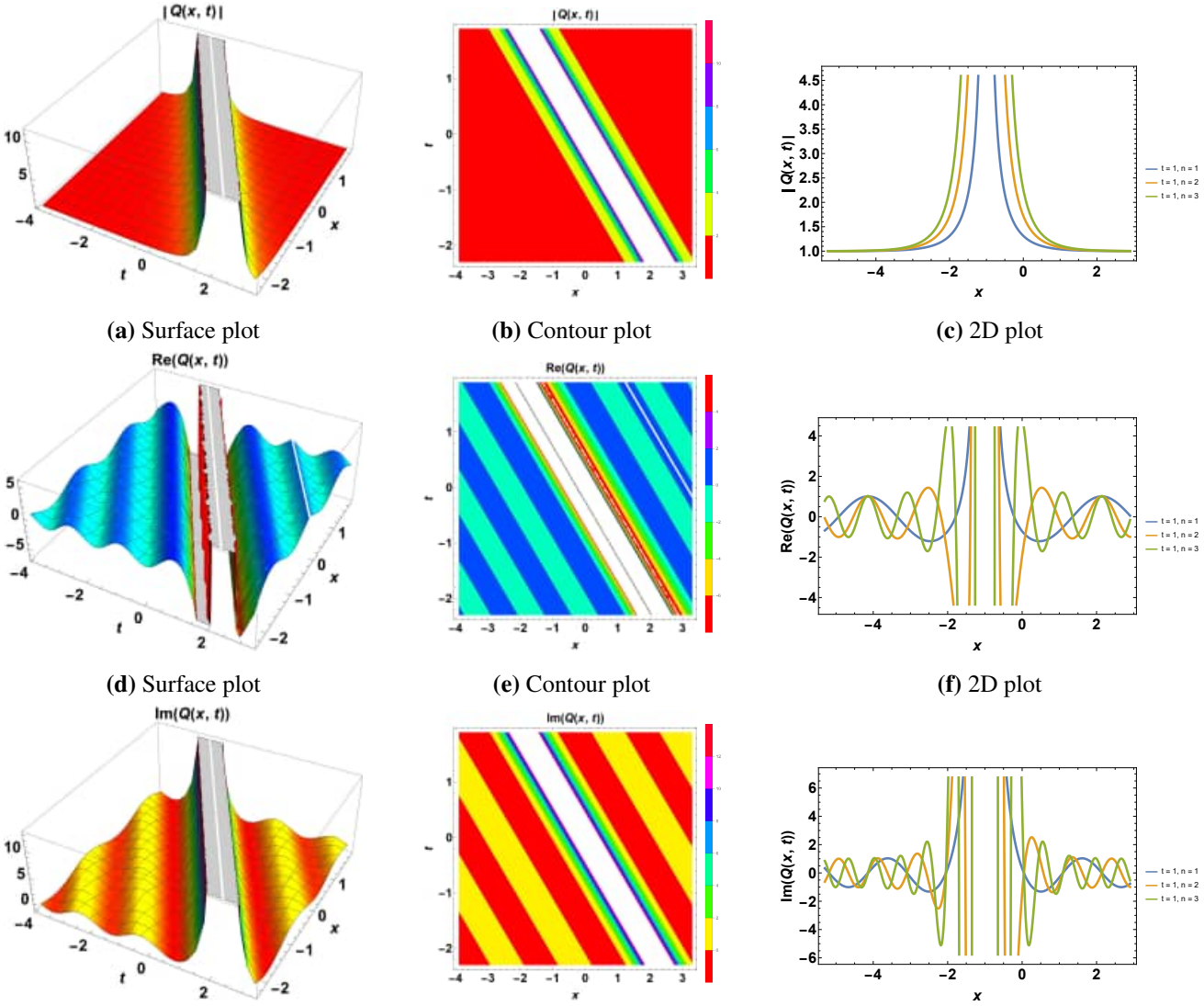

(a) Surface plot **(b)** Contour plot **(c)** 2D plot

(d) Surface plot **(e)** Contour plot **(f)** 2D plot

(g) Surface plot **(h)** Contour plot **(i)** 2D plot

Figure 12. Profile of a singular soliton given $n = 3$.

Figures 13–15 depict periodic solutions using the complex-valued solution (53). Unlike solitons, periodic solutions exhibit repeating structures over space. For $n = 1$ in Figure 13, the periodic nature of the solution is evident, with repeating peaks and troughs in the modulus, as shown in the surface plots (Figure 13(a), (d), and (g)). The contour plots (Figure 13(b), (e), and (h)) highlight the periodicity, and the 2D plots (Figure 13(c), (f), and (i)) confirm the regular structure of the solution. With $n = 2$ in Figure 14, the periodic peaks and troughs become more pronounced, as evidenced by the surface plots (Figure 14(a), (d), and (g)). The contour plots (Figure 14(b), (e), and (h)) show a sharper contrast between the peaks and troughs, and the 2D plots (Figure 14(c), (f), and (i)) confirm the enhancement of the periodic structure. In Figure 15, the periodic peaks and troughs are even more pronounced for $n = 3$, as shown in the surface plots (Figure 15(a), (d), and (g)). The contour plots (Figure 15(b), (e), and (h)) depict a highly regular pattern, and the 2D plots (Figure 15(c), (f), and (i)) confirm that the periodic structure becomes sharper with increased nonlinearity.

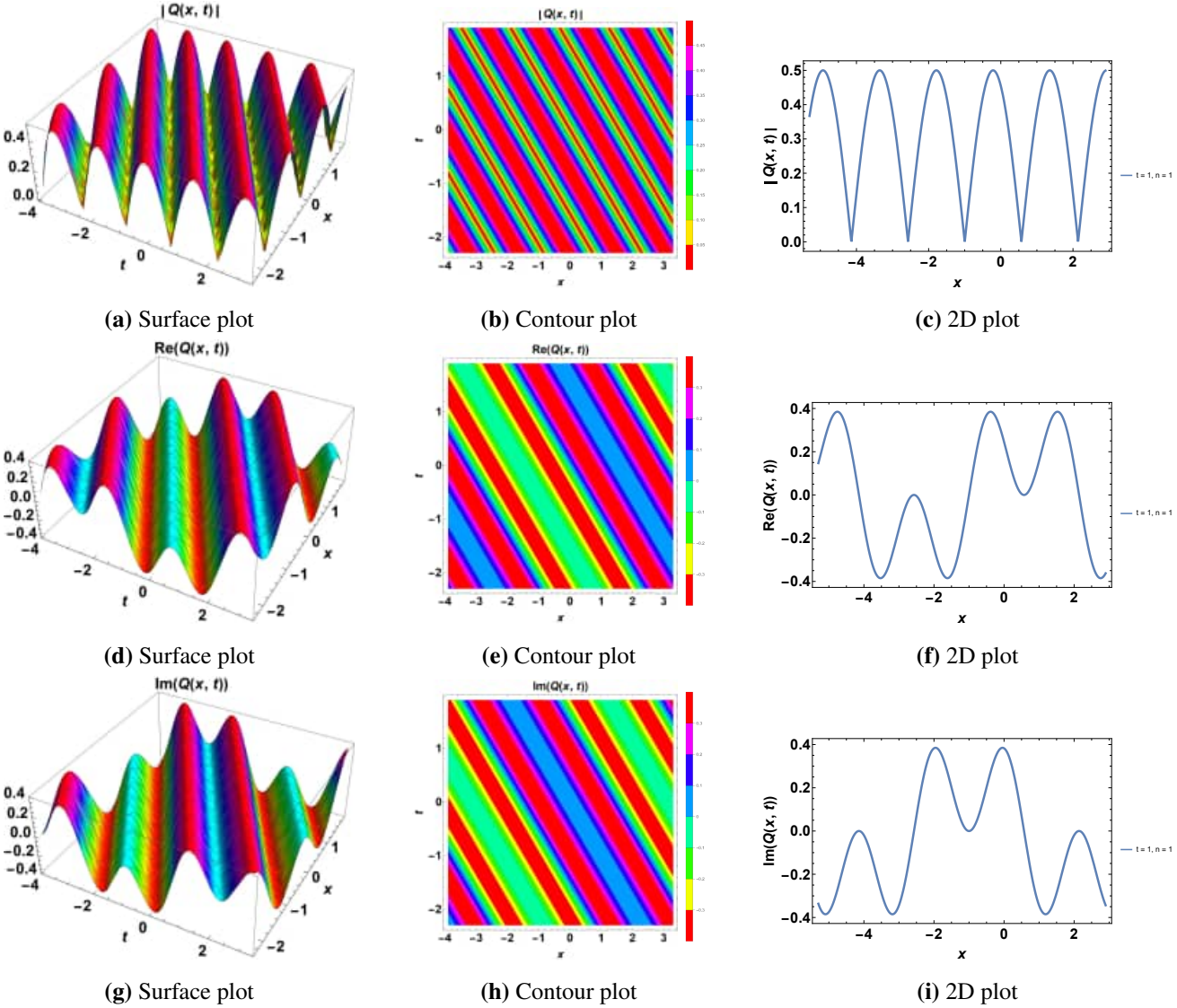

(a) Surface plot **(b)** Contour plot **(c)** 2D plot

(d) Surface plot **(e)** Contour plot **(f)** 2D plot

(g) Surface plot **(h)** Contour plot **(i)** 2D plot

Figure 13. Profile of a periodic solution given $n = 1$.

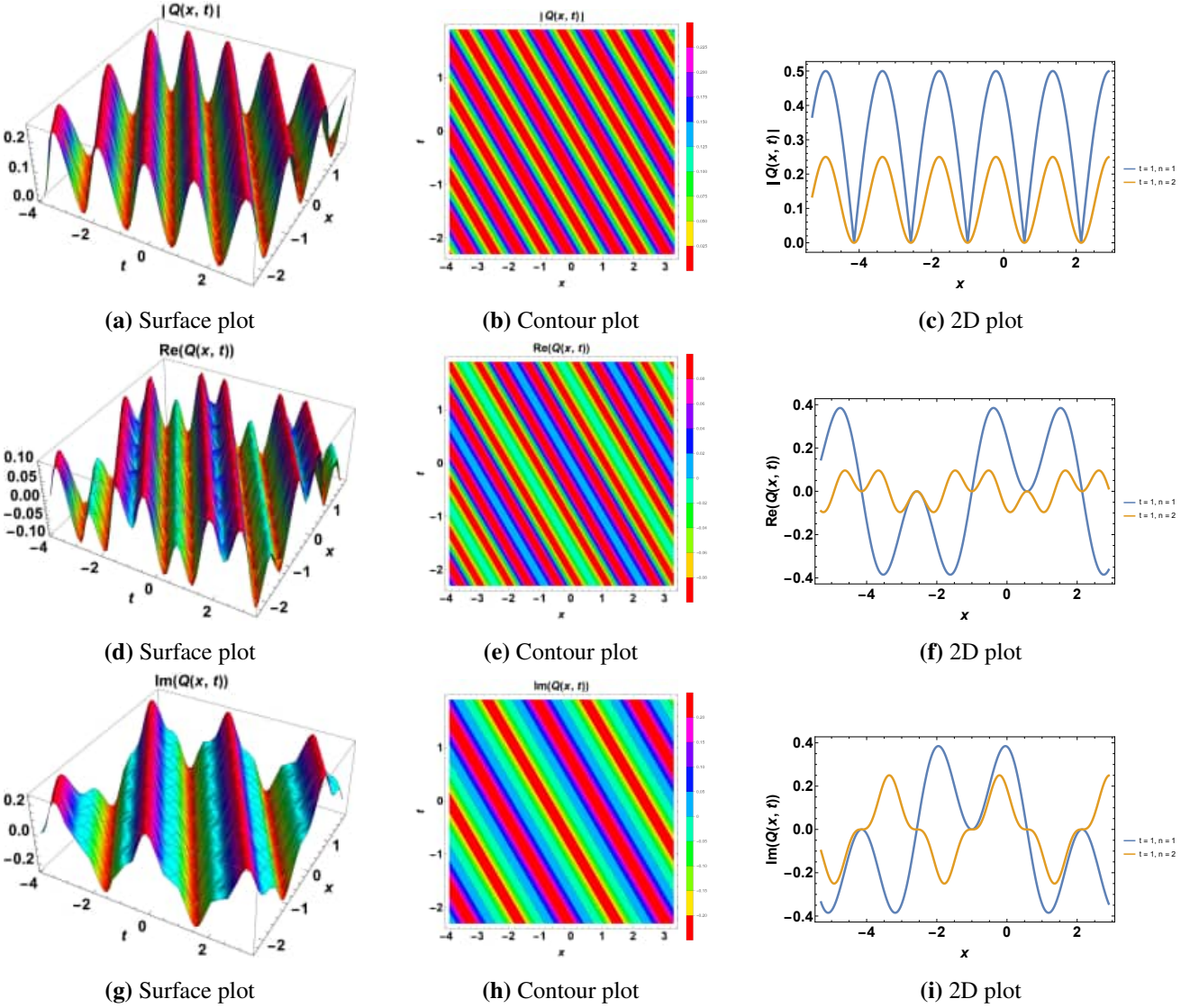

(a) Surface plot **(b)** Contour plot **(c)** 2D plot

(d) Surface plot **(e)** Contour plot **(f)** 2D plot

(g) Surface plot **(h)** Contour plot **(i)** 2D plot

Figure 14. Profile of a periodic solution given $n = 2$.

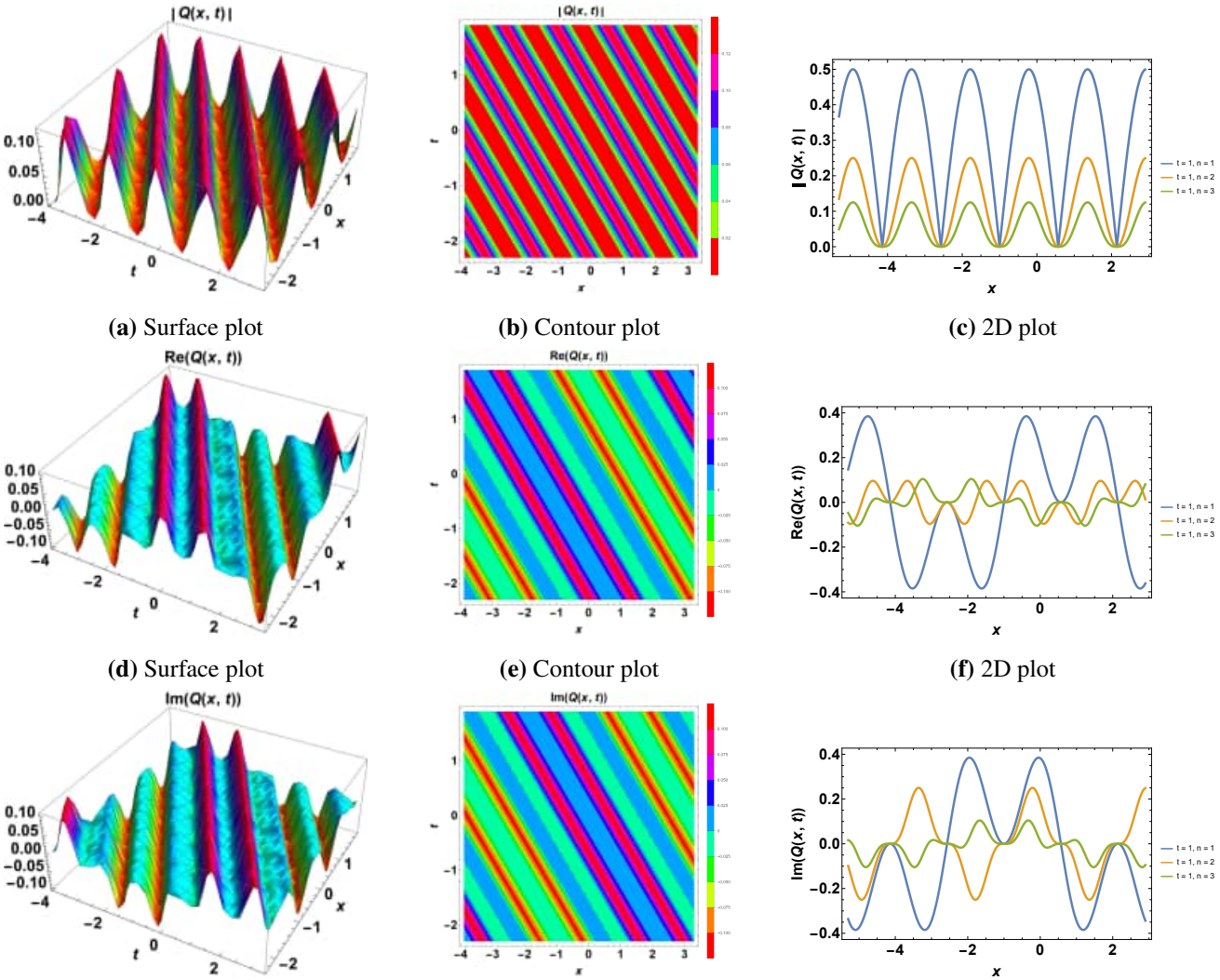

(a) Surface plot **(b)** Contour plot **(c)** 2D plot

(d) Surface plot **(e)** Contour plot **(f)** 2D plot

(g) Surface plot **(h)** Contour plot **(i)** 2D plot

Figure 15. Profile of a periodic solution given $n = 3$.

The behavior of soliton solutions across different types (bright solitons, singular solitons, dark solitons, and periodic solutions) shows distinct yet interconnected patterns as the power nonlinearity increases. This trend reveals important insights into how soliton dynamics are influenced by nonlinearity in optical systems. As the power nonlinearity increases, several key characteristics of the solitons are amplified, leading to sharper, more localized profiles, regardless of the type of soliton under consideration. The overall impact of increasing power nonlinearity on the different soliton types illustrates the diversity of behaviors that can be observed in nonlinear systems. While bright solitons become more concentrated and resistant to dispersion, singular solitons exhibit an extreme focusing of energy near their core, creating sharp, localized fields. Dark solitons, meanwhile, deepen their characteristic dips, maintaining stability in nonlinear environments, and periodic solutions sharpen and densify, leading to more regular and ordered wave patterns. This diversity of soliton behavior highlights the rich dynamics that arise from the interaction between dispersion, nonlinearity, and the initial conditions in these systems. Such a range of soliton solutions is essential for

understanding the complex behavior of nonlinear optical systems and the potential to control and manipulate these solutions for technological applications. For instance, bright solitons can be used for signal transmission in fiber optics, dark solitons for phase modulation, singular solitons for high-intensity beam generation, and periodic solutions for filtering and guiding light in photonic structures. The insights gained from the analysis of solitons' behavior with increasing power nonlinearity have significant implications for the design and optimization of nonlinear optical systems, including fiber optics, waveguides, and other systems involving nonlinear wave propagation. By understanding how solitons behave as a function of the nonlinearity parameter, engineers and physicists can better design systems to control solitons' propagation, stability, and interactions. This is crucial for the development of next-generation communication systems, where solitons are used to transmit information over long distances with minimal distortion, or in optical waveguides, where the precise control of light is necessary for applications such as switching, routing, and sensing. Furthermore, understanding the role of nonlinearity in shaping soliton profiles could also advance technologies in quantum communication, plasma physics, and nonlinear laser optics, where intense, localized fields are required to achieve specific outcomes.

In summary, the analysis of soliton behavior under varying power nonlinearity provides a comprehensive understanding of how these nonlinear waveforms evolve, offering valuable insights for future research and applications in nonlinear wave propagation and optical technologies.

6. Conclusions

As we draw to a close on this investigation, we reflect on the exhaustive examination conducted into the NLSE in the context of (3+1) dimensions. Our inquiry has been enriched by the incorporation of cross-spatio-dispersion and generalized Kudryashov's SPM through the utilization of the generalized Jacobi elliptic method. This amalgamation of methodologies has enabled a thorough exploration into the behavior of nonlinear waves in nonlinear media. Our primary objective throughout this study has been to derive new optical soliton solutions expressed through two main mathematical frameworks: Jacobi elliptic functions and Weierstrass elliptic functions. These solutions mark a significant leap forward in our comprehension of the intricate dynamics dictating wave propagation within nonlinear media. Importantly, the solutions we have obtained exhibit remarkable transformations contingent upon the parameter 'm'. This parameter governs the elliptic functions and plays a crucial role in shaping the behavior of the solutions. The spectrum of solutions we have uncovered is broad and enlightening. We have transitioned from optical bullet solutions, which are compact, localized wave packets resembling solitary waves, to optical domain wall solutions, characterized by abrupt changes in phase or amplitude across a distinct boundary. Singular soliton solutions, representing solitary waves that retain their shape and velocity during propagation, have also been elucidated. Finally, we have delved into the realm of Weierstrass elliptic functions, which are doubly periodic functions providing a rich mathematical framework for describing complex wave phenomena. These findings shed light on the intricate interplay among dispersion, nonlinearity, and self-modulation phenomena within optical systems. By unraveling these complexities, we gain deeper insights into the underlying mechanisms governing wave dynamics in nonlinear media. To enhance the clarity of our presentation and facilitate comprehension, we have provided comprehensive visualizations in 3D, 2D, and contour formats. These visual representations offer intuitive insights

into the structural attributes of the solutions, revealing patterns and behaviors that might otherwise be obscured by mathematical formalism alone. Furthermore, they highlight the potential applications of these solutions across various domains of physics, from understanding fundamental wave behavior to practical applications in fields such as optical communication and signal processing. In essence, our discoveries not only advance our fundamental understanding of light propagation within complex media but also hold promise for practical implications across a spectrum of disciplines. As we look ahead, these findings will undoubtedly serve as a catalyst for further research and innovation in critical areas of study, propelling us toward new frontiers in the understanding and manipulation of nonlinear wave phenomena.

Recent experimental developments suggest that our theoretical solutions may be realized in practice. Studies on ultrafast fiber lasers have demonstrated multi-wavelength soliton dynamics, soliton explosions, and chaotic soliton states, offering feasible platforms for validation [27]. The formation of soliton molecules via polarization-induced mechanisms further supports the relevance of our solutions in real-world systems [28]. Additionally, the existence of biperiodic pulsations and solitonic states in fiber lasers highlights another experimental framework where our analytical solutions may be validated, particularly in systems governed by a balance of dispersion and nonlinearity [29]. The use of deep learning for dynamic modeling and coded information storage of vector soliton pulsations in mode-locked fiber lasers [30], as well as the development of tunable three-wavelength fiber lasers with transient switching between soliton and q-switched mode-locked states [31], further demonstrate the potential for experimental realization. Additionally, the generation and π-phase-induced oscillations of multi soliton molecular complexes in ultrafast fiber lasers based on MOF-253@Au provide another avenue for observing and controlling soliton interactions [32].

Author contributions

Nafissa Toureche Trouba: Writing – original draft; Mohamed E. M. Alngar: Writing – original draft; Reham M. A. Shohib: Writing – original draft; Haitham A. Mahmoud: Writing – review & editing; Yakup Yildirim: Writing – review & editing; Huiying Xu: Writing – review & editing; Xinzhong Zhu: Project administration. All authors have read and agreed to the published version of the manuscript.

Use of Generative-AI tools declaration

The authors declare that they have not used Artificial Intelligence tools in the creation of this article.

Acknowledgments

The authors extend their appreciation to King Saud University for funding this work through the Researchers Supporting Project (number RSPD2025R1006), King Saud University, Riyadh, Saudi Arabia.

This work was supported by the National Natural Science Foundation of China (62376252), the Key Project of Natural Science Foundation of Zhejiang Province (LZ22F030003), and Zhejiang Province Leading Geese Plan (2024C02G1123882, 2024C01SA100795).

Conflict of interest

All authors declare no conflicts of interest in this paper.

References

1. A. Biswas, Theory of optical bullets- Abstract, *J. Electromagnet. Wave.*, **16** (2002), 419–420. https://doi.org/10.1163/156939302X01254
2. A. Djazet, C. B. Tabi, S. I. Fewo, T. C. Kofane, Vector dissipative light bullets in optical laser beam, *Appl. Phys. B*, **126** (2020), 74. https://doi.org/10.1007/s00340-020-07422-7
3. K. S. Al-Ghafri, E. V. Krishnan, S. Khan, A. Biswas, Optical bullets and their modulational instability analysis, *Appl. Sci.*, **12** (2022), 9221. https://doi.org/10.3390/app12189221
4. T. Vachaspati, *Kinks and Domain Walls: An introduction to classical and quantum solitons*, Cambridge: Cambridge University Press, 2006. https://doi.org/10.1017/CBO9780511535192
5. N. A. Kudryashov, Hamiltonians of the generalized nonlinear Schrödinger equations, *Mathematics*, **11** (2023), 2304. https://doi.org/10.3390/math11102304
6. N. A. Kudryashov, Mathematical model with unrestricted dispersion and polynomial nonlinearity, *Appl. Math. Lett.*, **138** (2023), 108519. https://doi.org/10.1016/j.aml.2022.108519
7. N. A. Kudryashov, Mathematical model of propagation pulse in optical fiber with power nonlinearities, *Optik*, **212** (2020), 164750. https://doi.org/10.1016/j.ijleo.2020.164750
8. N. A. Kudryashov, A generalized model for description of propagation pulses in optical fiber, *Optik*, **189** (2019), 42–52. https://doi.org/10.1016/j.ijleo.2019.05.069
9. N. A, Kudryashov, E. V. Antonova, Solitary waves of equation for propagation pulse with power nonlinearities, *Optik*, **217** (2020), 164881. https://doi.org/10.1016/j.ijleo.2020.164881
10. W. X. Qiu, Z. Z. Si, D. S. Mou, C. Q. Dai, J. T. Li, W. Liu, Data-driven vector degenerate and nondegenerate solitons of coupled nonlocal nonlinear Schrödinger equation via improved PINN algorithm, *Nonlinear Dyn.*, **113** (2025), 4063–4076. https://doi.org/10.1007/s11071-024-09648-y
11. K. L. Geng, D. S. Mou, C. Q. Dai, Nondegenerate solitons of 2-coupled mixed derivative nonlinear Schrödinger equations, *Nonlinear Dyn.*, **111** (2023), 603–617. https://doi.org/10.1007/s11071-022-07833-5
12. D. S. Mou, Z. Z. Si, W. X. Qiu, C. Q. Dai, Optical soliton formation and dynamic characteristics in photonic Moiré lattices, *Opt. Laser Technol.*, **181** (2025), 111774. https://doi.org/10.1016/j.optlastec.2024.111774
13. X. K. Wen, G. Z. Wu, W. Liu, C. Q. Dai, Dynamics of diverse data-driven solitons for the three-component coupled nonlinear Schrödinger model by the MPS-PINN method, *Nonlinear Dyn.*, **109** (2022), 3041–3050. https://doi.org/10.1007/s11071-022-07583-4
14. J. G. Liu, W. H. Zhu, Multiple rogue wave, breather wave and interaction solutions of a generalized (3+1)-dimensional variable-coefficient nonlinear wave equation, *Nonlinear Dyn.*, **103** (2021), 1841–1850. https://doi.org/10.1007/s11071-020-06186-1

15. G. Wang, X. Wang, T. Huang, Explicit soliton solutions of (3+1)-dimensional nonlinear Schrödinger equation with time variable coefficients, *Optik*, **275** (2023), 170628. https://doi.org/10.1016/j.ijleo.2023.170628

16. G. Wang, X. Wang, F. Guan, H. Song, Exact solutions of an extended (3+1)-dimensional nonlinear Schrödinger equation with cubic-quintic nonlinearity term, *Optik*, **279** (2023), 170768. https://doi.org/10.1016/j.ijleo.2023.170768

17. B. Gao, Y. Wang, Complex wave solutions described by a (3+1)-dimensional coupled nonlinear Schrödinger equation with variable coefficients, *Optik*, **227** (2021), 166029. https://doi.org/10.1016/j.ijleo.2020.166029

18. G. Wang, A novel (3+1)-dimensional sine-Gorden and a sinh-Gorden equation: Derivation, symmetries and conservation laws, *Appl. Math. Lett.*, **113** (2021), 106768. https://doi.org/10.1016/j.aml.2020.106768

19. A. M. Wazwaz, M. Abu Hammad, S. A. El-Tantawy, Bright and dark optical solitons for (3+1)-dimensional hyperbolic nonlinear Schrödinger equation using a variety of distinct schemes, *Optik*, **270** (2022), 170043. https://doi.org/10.1016/j.ijleo.2022.170043

20. A. M. Elsherbeny, M. Mirzazadeh, A. H. Arnous, A. Biswas, Y. Yildirim, A. Dakova, A. Asiri, Optical bullets and domain walls with cross spatio-dispersion and having Kudryashov's form of self-phase modulation, *Contemp. Math.*, **4** (2023), 505–517. https://doi.org/10.37256/cm.4320233359

21. H. Ur Rehman, I. Iqbal, M. Mirzazadeh, M. S. Hashemi, A. U. Awan, A. M. Hassan, Optical solitons of new extended (3+1)-dimensional nonlinear Kudryashov's equation via ϕ^6-model expansion method, *Opt. Quantum Electron.*, **56** (2024), 279. https://doi.org/10.1007/s11082-023-05850-1

22. A. M. Elsherbeny, M. Mirzazadeh, A. H. Arnous, A. Biswas, Y. Yıldırım, A. Asiri, Optical bullets and domain walls with cross-spatio dispersion having parabolic law of nonlinear refractive index, *J. Opt.*, 2023. https://doi.org/10.1007/s12596-023-01398-1

23. M. Ekici, A. Sonmezoglu, A. Biswas, Stationary optical solitons with Kudryashov's laws of refractive index, *Chaos Soliton. Fract.*, **151** (2021), 111226. https://doi.org/10.1016/j.chaos.2021.111226

24. H. Esen, A. Secer, M. Ozisik, M. Bayram, Analytical soliton solutions of the higher order cubic-quintic nonlinear Schrödinger equation and the influence of the model's parameters, *J. Appl. Phys.*, **132** (2022), 053103. https://doi.org/10.1063/5.0100433

25. A. T. Ali, New generalized Jacobi elliptic function rational expansion method, *J. Comput. Appl. Math.*, **235** (2011), 4117–4127. https://doi.org/10.1016/j.cam.2011.03.002

26. E. M. E. Zayed, M. E. M. Alngar, Optical solitons in birefringent fibers with Biswas–Arshed model by generalized Jacobi elliptic function expansion method, *Optik*, **203** (2020), 163922. https://doi.org/10.1016/j.ijleo.2019.163922

27. Z. Z. Si, Y. Y. Wang, C. Q. Dai, Switching, explosion, and chaos of multi-wavelength soliton states in ultrafast fiber lasers, *Sci. China Phys. Mech. Astron.*, **67** (2024), 274211. https://doi.org/10.1007/s11433-023-2365-7

28. Z. Z. Si, Z. T. Ju, L. F. Ren, X. P. Wang, B. A. Malomed, C. Q. Dai, Polarization-induced buildup and switching mechanisms for soliton molecules composed of noise-like-pulse transition states, *Laser Photon. Rev.*, **19** (2025), 2401019. https://doi.org/10.1002/lpor.202401019

29. Z. T. Ju, Z. Z. Si, X. Yan, C. Q. Dai, Solitons and their biperiodic pulsation in ultrafast fiber lasers based on CB/GO, *Chinese. Phys. Lett.*, **41** (2024), 084203. https://doi.org/10.1088/0256-307X/41/8/084203

30. Z. Z. Si, D. L. Wang, B. W. Zhu, Z. T. Ju, X. P. Wang, W. Liu, et al., Deep learning for dynamic modeling and coded information storage of vector-soliton pulsations in mode-locked fiber lasers, *Laser Photon. Rev.*, **18** (2024), 2400097. https://doi.org/10.1002/lpor.202400097

31. Z. Z. Si, C. Q. Dai, W. Liu, Tunable three-wavelength fiber laser and transient switching between three-wavelength soliton and Q-switched mode-locked states, *Chin. Phys. Lett.*, **41** (2024), 020502. https://doi.org/10.1088/0256-307X/41/2/020502

32. Z. Z. Si, L. F. Ren, D. L. Wang, Z. T. Ju, X. P. Wang, Y. Y. Wang, et al., Generation and π-phase-induced oscillations of multi-soliton molecular complexes in ultrafast fiber lasers based on MOF-253@Au, *Chem. Eng. J.*, **505** (2025) 159024. https://doi.org/10.1016/j.cej.2024.159024

AIMS Press